INSIGHT

"ImplementatioN in real SOFC Systems of monItoring and diaGnostic tools using signal analysis to increase tHeir lifeTime"

Grant Agreement n° 735918 –
Research and Innovation Project

Deliverable D4.1 State-of-Art on EIS, THD as Diagnostic Tools for SOFC Status Evaluation

Start date of the project: 1st January 2017
Duration: 36 months
Project Coordinator: Julie MOUGIN – CEA

Contact: Julie MOUGIN – CEA LITEN France - julie.mougin@cea.fr

Document Classification

Title	State-of-Art on EIS, THD as Diagnostic Tools for SOFC Status Evaluation
Deliverable	D4.1
Reporting Period:	1
Date of Delivery foreseen	Project Month 7 AND DATE 30/07/2017
Actual Date of Delivery	27/12/2017
Validation date	24/01/2018

Authors	Jan Pieter Ouweltjes (HTc), Alexandra Ploner (DTU), Priscilla Caliandro (EPFL), Arata Nakajo (EPFL), Jan Van Herle (EPFL), Dani Juricic (IJS), Bertrand Morel (CEA), Marco Gallo (UNISA), Pierpaolo Polverino (UNISA), Stefan Pofahl (AVL)
Work package	WP 4 – Monitoring and Diagnostic Tools
Dissemination	PU
Nature	R: Document, report
Version	*V*1.5
Doc ID Code	D4.1_INSIGHT_P7_AVL_160617
Keywords	EIS, THDA, Monitoring, SOFC, Diagnosis

Document History

Partner	Remark	Version	Date
P7 AVL	Draft	V1.0	13/06/2017
P7 AVL	Pre-Final	V1.1	27/12/2017
P9 HTc	Check	V1.2	27/12/2017
P3 UNISA	Clarifications	V1.3	12/01/2018
P9 HTc	Minor	V1.4	15/01/2018
P7 AVL	Final	V1.5	18/01/2018

Document Validation

Partner	Approval (Signature or e-mail reference)
P1 - CEA	Julie Mougin, Approved 24/01/2018

This project has received funding from the Fuel Cells and Hydrogen 2 Joint Undertaking under grant agreement No 735918. This Joint Undertaking receives support from the European Union's Horizon 2020 research and innovation programme and Hydrogen Europe and N.ERGHY

Document Abstract

The document summarizes on the state of the art on the topics EIS and THDA as a diagnostic tool for SOFC systems.

Table of Contents

Abbreviations

ADAS	Advanced Driver Assistance Systems
AFM	Atomic Force Microscopy
ALS	Adler-Lane-Steele
ANN	Artificial neural networks
ASC	Anode Supported Cell
ASR	Area Specific Resistance
BoP	Balance of Plant
DFT	Density functional theory
DRT	Distribution of Relaxation Times
EDX	Energy Dispersion X-ray
EIS	Electrochemical Impedance Spectroscopy
EMF	Electromotive Force
ESC	Electrolyte Supported Cell
FESEM	Field Emission Scanning Electron Microscopy
FIB	Focused Ion Beam
GDC	Gadolinium doped Ceria
ICP-OES	Induced coupled plasma-Optic Emission Spectroscopy
LSCF	Lanthanum strontium cobalt ferrite
MIC	Metallic Interconnect
MIEC	Mixed Ionic and Electronic conductor
ORR	Oxygen Reduction Reaction
ScSZ	Scandia stabilized Zirconia
SDC	Scandia doped Ceria
SEM	Scanning Electron Microscopy
SoH	State of Health
TEM	Transmission Electron Microscopy
THD	Total Harmonic Distortion
TPX	Temperature Programmed
TXRF	Total Reflection X-ray fluorescence
WDS	Wavelength dispersive spectroscopy
XRD	X-ray Diffraction
YSZ	Yttrium stabilized Zirconia

1. Literature survey on SOFC monitoring relevant topics

1.1. Characterization of Fuel Cell Stacks and Classification on Monitoring Approaches

UNISA, Marco Gallo, Pierpaolo Polverino

To support the successful deployment of fuel cells, specific diagnostic methods are needed for both stack and balance-of-plant (BoP) components with the objective of having meaningful information on the actual State-of-Health (SoH) of the entire system in real-time. A holistic view can guarantee an advanced management and a comprehensive solution to the problem of achieving improved performance, maintenance scheduling, higher reliability and thus increased lifetime of the system.

Fuel cell operations are influenced by several physical phenomena occurring inside the cell. Abnormal operating conditions may introduce system faults and worse degradation mechanisms. These critical behaviors force the research activities to develop new monitoring and diagnosis techniques to ensure optimal system management and improve fuel cell performance and durability [1]. Fault diagnosis consists in the determination of fault type, size, location and time of detection (when possible). The diagnostic procedure is based on the observed analytical and heuristic symptoms and the heuristic knowledge of the process. Particularly, three main processes are required as shown in Figure 1: data acquisition and treatment, fault detection and isolation (FDI).

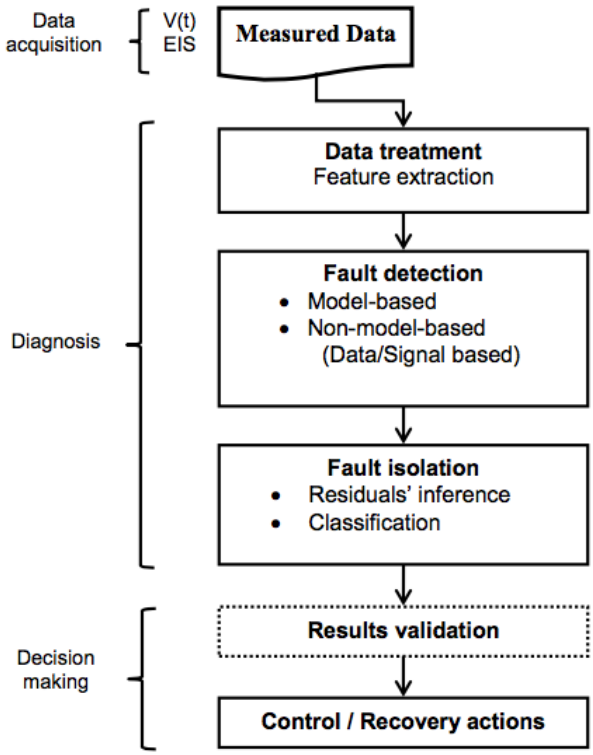

Figure 1 - Steps for diagnostic tool development (adapted from [2]).

A suitable diagnostic tool aims at identifying the system faults in real time. Indeed, even if some faults are quite easy to detect, their isolation is sometimes hard to perform and requires detailed information. Fault detection is based on the on-line comparison between measured data and reference ones evaluated in normal system behavior [2].

In parallel with system diagnosis, researches are also focusing on Prognostic and Health Management (PHM) activities [3]. These studies are mainly aimed to evaluate the system remaining useful life (RUL) studying the system ageing, planning recovery action and then, reducing the risk of failures.

Particularly, PHM is oriented to predict the voltage degradation depending on the history of the system mission profile. The system response evolution caused by ageing is a sensible point to consider in diagnosis algorithms development.

1.1.1. Fuel cells monitoring

Fuel cells monitoring is usually achieved by observing their electrical behavior under different operating conditions. The most used methods to characterize the fuel cell performance are based on electrochemical techniques, namely polarization curves, Cyclic Voltammetry (CV), Electrochemical Impedance Spectroscopy (EIS), current sweeps, current interruption, etc.

1.1.1.1. Polarization curves

The durability of fuel cells is significantly affected by several degradation mechanisms, which reduce cell performance during time and can lead to stack failures. Methods to directly observe degradation phenomena aiming at the evaluation of loss of performances and measure their behavior over time are difficult to implement. Usually, indirect SoH indicators, related to the decay of the voltage over time and coupled with temperature and current density are adopted [4]. Indeed, the effect of operating parameters, as temperature, voltage and current density has been studied in literature. For instance, as it concerns SOFC, Nakajo et al. [5] investigated the distribution and the evolution of the performance losses under practical operating conditions by means of VI characterizations performed at fixed operating times. Zaccaria et al. [6] developed a simplified real-time model of degradation relating the voltage degradation rate per 1000 h of operation to current density, fuel utilization and temperature, by increasing the ohmic resistance. After 12000 h of continuous work, they measured a reduction in the cell voltage of about 12% and a growth in the total amount of thermal effluent to the air of about 15% [7]. Yan et al. [8] investigated the degradation of the SOFC for more than 750 h under a fixed current density in order to evaluate the behavior of the cells and detrimental mechanisms, which might lead to cell performance losses. Post-test examination related the degradation to three main phenomena: contact decaying leading to an increasing in the Area Specific Resistance (ASR), stainless steel interconnect oxidation, especially at high current densities, and stack leakage, which contributed to most of the stack degradation. Further details can be found in [9] and [10].

1.1.1.2. Electrochemical Impedance Spectroscopy

Among fuel cell characterization methods aiming at monitoring performance behavior, Electrochemical Impedance Spectroscopy (EIS) is proved one of the most powerful techniques able to investigate the main phenomena occurring in electrochemical cells (PEMFC, SOFC, Li-ion batteries, etc.) for online prognostic purposes and SoH monitoring thanks to non-invasive features [11].

EIS provides a wealth of information about the analyzed system. It is a non-destructive tool extremely useful to give an insight on the SoH of the cell and to evaluate how a degradation process could affect the overall performance losses [12]. Moreover, it allows detecting the occurrence of incipient faults several minutes before they evidently arise [13]. Indeed, this method allows analyzing electrochemical reactions, charge and mass transfer as well as thermal phenomena for a single cell, a Single Repeated Unit (SRU) or a complete stack [14].

An overview can be found in [15], where Huang et al. investigated 150 journal papers dealing with AC impedance modelling for SOFC diagnosis. Nechache et al. [16] showed how EIS can be applied to Solid Oxide Electrolyser Cell (SOEC) systems to characterize performance mechanisms, study the degradation mechanisms for different cell configurations and monitoring overall SOEC performances for diagnostic applications. Nechache et al. [17] combined EIS, polarization curve and deconvolution technique to analyze SOEC technology and study the electrochemical behavior of commercial cells.

They proved that these methodologies represent a key-tool for monitoring in-situ performances and elaborate control-aided strategies.
With respect to Polymer Electrolyte Membrane Fuel Cells (PEMFCs) EIS-Based diagnosis, Petrone et al. [11] presented a detailed review on model-based diagnosis methodology, focusing on Equivalent Circuit Modelling (ECM) derived from EIS data and aiming at reaching a good compromise between accuracy and efforts in computation, extremely needed for on-board applications.

Several approaches are exploited to extract from EIS measurements specific features able to detect and isolate undesired events in fuel cells. Among them, ECM correlates specific circuit components to the investigated physical phenomena. This aspect represents the main advantage of combining EIS with ECM, since suitable impedance contributors (e.g., ohmic resistance, charge-transfer resistance, etc.) can be identified by analyzing circuit parameters [18]. From the evaluation of the ECM parameters, it is possible to discern between normal and faulty conditions [19]. It is worth remarking that the choice of the most effective ECM is related to the type of fault to be detected. However, to develop flexible and generalizable diagnostic tools, it is preferable to employ comprehensive ECM able to account for a large number of possible faults and different kind of system configurations (as the model proposed in Figure 2).

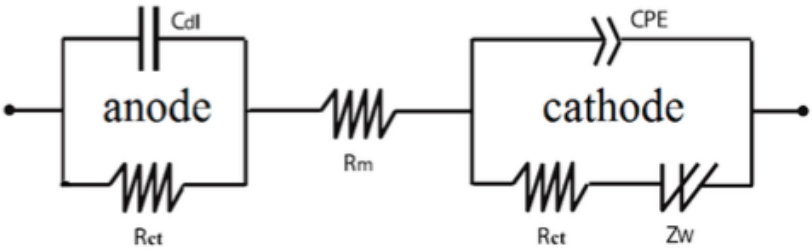

Figure 2 – Exemplary scheme of an Equivalent Circuit Model (taken from [20]).

Electrical elements used for the impedance modelling are clearly described by Khan and Rizvi [21], who proposed ECMs for diverse kinds of SOFC cathode materials.

Hissel and Perà [22] summed up recent developments and experimentations in efficient diagnostic and SoH estimation methodologies. Although the literature concerning EIS is vast, only few works seek to investigate monitoring and diagnosis approaches for SOFC technologies involving EIS. For this reason, great attention should be given to diagnostic methodologies derived from impedance measurements, which allows testing the system in real-time in a non-invasive way, to develop an online diagnostic tool for SOFC.

In the work of Barelli at al. [23], the authors performed a literature survey on failure causes and relative diagnostic systems for SOFC technologies. The main degradation phenomena occurring during SOFCs normal operation have been analyzed. Similarly, Lee et al. [24] investigated mechanisms and symptoms of several simulated failure modes, especially fuel starvation, air-depletion and wet and dry cycling modes.
Monitoring the behavior of a technology requires a complete knowledge about in-situ phenomena occurring in the cell, and how they are related to electric parameters, which might be derived from the EIS measurements. Sometimes, when experimental campaigns lack of information, physical model represents the correct approach to simulate the real fuel cell behavior. For these reasons,

Hofmann and Panopoulos [25] developed a mathematical model for planar SOFC to simulate steady state performance characteristics and in particular to simulate electrochemical impedance. The model was applied in a detailed parametric analysis of the losses in order to deconvolute the impedance spectrum, by relating each main transport process to an impedance arc. Parametric analysis of EIS was performed by varying characteristic parameters as porosity, tortuosity, anode thickness, anodic exchange current density and so on. Similarly, Zhu et al. [26] investigated through modelling approach the influences of detailed surface chemistry within SOFC composite anode structures on EIS. By developing a 6-elements ECM based on physical parameter models, they computed qualitative trends of frequency shifts measured on the complex impedance of SOFCs operating on hydrogen, carbon monoxide and syngas mixtures. On the same line, Fadaei and Mohammadi [27] exploited physical models to perform a parametric study on the effects of overvoltage, inlet fuel concentration, temperature, anode thickness, inflow velocity and porosity on the impedance spectrum. Lang et al. [28] tested SOFC short stacks with sintered anode-supported cells and identified the nature of losses by fitting the impedance spectra to an ECM based on five elements. Finally, Montinaro et al. [29] tested an SOFC with Lanthanum Strontium Cobalt Ferrite (LSCF) cathode at different operating conditions (e.g., changing gas partial pressure or cell temperature, inducing H_2S poisoning, etc.) through EIS, in order to identify the main mechanisms contributing to the polarization resistance, especially at the anode side. In particular, they presented the evolution of VI curves and Nyquist plots under different conditions of S/C ratio, H_2S poisoning, voltage and raw materials.

In conclusion, it is worth remarking that EIS technique is a key tool to monitor the behavior of the polarization losses during time, to identify the causes of system degradation. This application, fast and non-invasive, might represent the basis to implement a fault detection and identification process on-board. The main issue is to correlate what emerges from impedance spectroscopy to the physical phenomena occurring in the system, to extract significant parameters to be monitored. Their deviation over well-defined thresholds cause the arising of an alarm that could lead to the identification of a fault. To do so, a diagnostic algorithm has to be coupled with EIS monitoring approaches.

1.1.2. Diagnosis: Model based approaches

Two main approaches are commonly exploited: non-model based and model based approaches. In the former approach, the fault information is obtained through heuristic knowledge (data-based) or signal processing (signal-based) or a combination of them [30]. In the latter one, the diagnosis is performed by evaluating the residuals between the experimental data and the model outputs [11]. Subsequently an inference analysis is done to detect the possible abnormal behavior and isolate the fault origins. Model-based methodologies usually rely in parameter estimation, parity equation or state observers approaches [2].

The *parameters-identification-based methods* are based on the identification of specific parameters usually related to the physical phenomena. The parameters are estimated during normal and faulty operating conditions to build a set of suitable parameter sets. These sets could be distinguished by applying suitable threshold levels. If one parameter, or its related residual (i.e. the difference between the considered parameter and a reference value), overcomes these thresholds, it can be assumed that the operating condition under investigation does not apply to the reference case (i.e. an abnormal or faulty state is occurring [32] – see Figure 3).

In *observer-based method*, the physical variables that characterize the problem are observed during the system operation to get a set of reliable residuals values, for instance, obtained from a suitable set of non-linear model equations related to a specific fault. Through this approach, fault detection is achieved when one variable overcomes the thresholds, and fault identification is fulfilled by comparing the obtained results with specific references [33].

In *parity space methods*, complex physical problems are usually simplified and linearized by employing a parity space linear domain for residuals calculation [34]. The application of these methods generates many residuals and only a certain number of them can be exploited for diagnosis. Although these approaches are still under development, they are considered quite promising for future improvement in fault diagnosis. The advantage of these methodologies consists in their subspace framework, presented in form of linear algebraic equations.

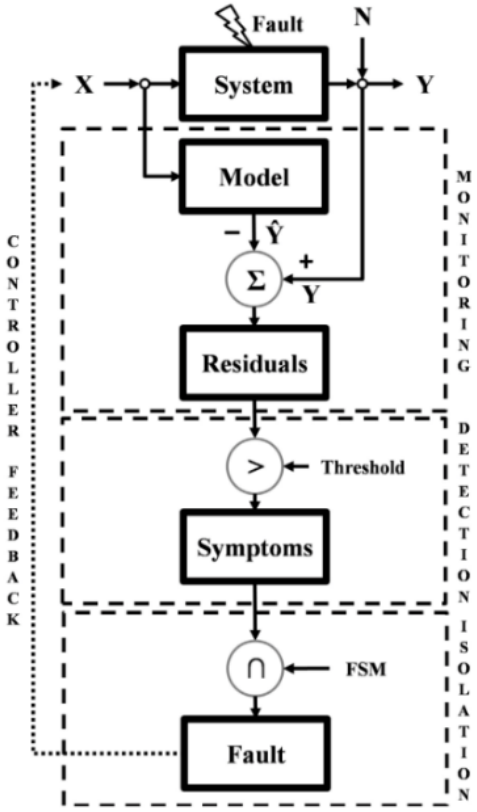

Figure 3 Example of the model based diagnosis scheme. Taken from [32]

Depending on the level of the required physical knowledge, the developed models are classified as: white-box (theoretical analytical models), black-box (such as artificial intelligence and statistical models) and grey-box (hybrid models). In general, for on-line diagnosis, grey- and black-box models are usually adopted.

1.1.2.1. White-box models

White-box models deeply rely on physical knowledge and are adopted to model electrochemical, thermal and fluid-dynamic phenomena (for instance, Nernst-Planck, Butler-Volmer and Fick's laws). From a computational point of view, they are very time consuming since they require solving complex partial-differential equations. Moreover, these models involve several parameters, often difficult to estimate.

1.1.2.2. Black-box models

The use of black-box models to compute residuals and carry out fault diagnosis allows to directly characterize the model parameters through the interpolation of training datasets rather than identification methods. Among others, artificial intelligence and heuristic techniques are often used. Artificial neural networks (ANN) are sometimes adopted in non-linear dynamic modelling [35]. This methodology implies a preliminary training process that needs a large amount of data to ensure good reliability. In case of PEMFC flooding diagnosis, residuals analysis is obtained from the comparison

between experimental and estimated pressure drop, obtained, in turn, by exploiting the neural networks trained with flooding-free data [35].
Moreover, the fuzzy logic (FL) methodology is very promising (especially for flooding conditions in PEMFC), but the online adjustment in case of new faults, not considered in the a priori fuzzy rules, is difficult to achieve [11].

1.1.2.3. Grey-box models

Grey-box models represent the trade-off between white- and black-box model, combining, on one hand, physical knowledge and, on the other hand, empirical formula or artificial intelligence structures. These models allow reaching good accuracy and genericity, even for non-linear phenomena. The grey-box models used for on-line faults detection and isolation are usually divided into parameters- identification-based, observed-based and parity space methods [31].

1.1.3. Diagnosis: Non-model based approaches

Non-model based methodologies are mainly related to data/knowledge-based (artificial intelligence and statistical methods) and signal-based, as summarized in Figure 4 [11].

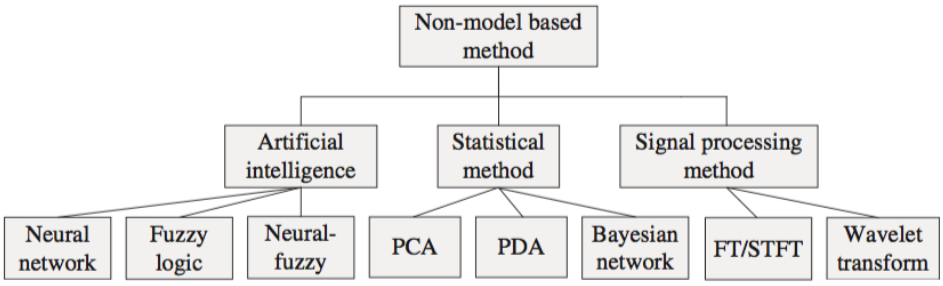

Figure 4 Non-model based techniques (taken from [11]).

Artificial intelligence (AI) methods allow the fault pattern recognition without system structure knowledge (physical model). To this purpose, the faults specific patterns are resumed in relevant features which are commonly classified in a feature hyperspace depending on the system state of health (normal/faulty conditions). The different approaches suggested for PEMFC on-line diagnosis applications based on both voltage and EIS measurements inputs are Artificial Neural-Networks (ANN), Fuzzy-Logic (FL), Adaptive Neuro-Fuzzy Inference Systems (ANFIS) and, recently, Visual-Block fuzzy inductive reasoning (Visual-Block FIR). Particularly this class can be very promising for fault isolation/classification if discriminating features are considered. Consequently, ANN, FL and ANFIS methods are mainly introduced for clustering technique applications.
On the contrary, methods based on probability theories can allow the variables dimension reduction, converting the correlated variables into a small number of uncorrelated features due to a huge amount of data and to their high level of correlation [11]. Principle component analysis (PCA) and Fischer discriminant analysis (FDA) are commonly used in case of linear correlation among the variables. While for variables non-linear features Kernel-PCA (KPCA) and KFDA are preferred. Bayesian networks (BN) probabilistic graphical models are also used for high uncertainty problems and problematic reasoning and decision making [36]. An interesting new data-based diagnostic strategy is presented in Li et al. in [37] combining FDA and spherical-shaped multiple-class support vector machine (SSM-SVM) approaches to extract features from single cell voltages.
Furthermore, the faults occurrence can be also detected exploiting signal processing methods. These methods are mainly oriented in signal analysis in frequency domain in order to exploit information that are not available in time domain. In PEMFC domain, stack/cell voltage and pressure drop signals are the most frequently exploited [1]. The main approaches commonly involved in PEMFC signal-

based diagnosis are the fast Fourier transform (FFT), used for stationary signal analysis [38] and the wavelet transform (WT) for non-stationary conditions [39]. Finally, a novel signal-based diagnosis approach is recently proposed by Damour et al. [40] for PEMFC applications. Authors introduces the empirical mode decomposition (EMD) technique to detect and isolate flooding and drying faults though the stack output voltage signal decomposition.

1.1.4. Bibliography

[1] Petrone, R. (2014). Electrochemical Impedance Spectroscopy for the on-board diagnosis of PEMFC via on-line identification of Equivalent Circuit Model parameters.

[2] Cadet, C., Jemeï, S., Druart, F., & Hissel, D. (2014). Diagnostic tools for PEMFCs: from conception to implementation. *International Journal of Hydrogen Energy*, 39(20), 10613-10626.

[3] Jouin, M., Gouriveau, R., Hissel, D., Péra, M. C., & Zerhouni, N. (2014). Prognostics of PEM fuel cell in a particle filtering framework. *International Journal of Hydrogen Energy*, 39(1), 481-494

[4] Guida, M., Postiglione, F., Pulcini, G. (2015). A random-effects model for long-term degradation analysis of solid oxide fuel cells. *Reliability Engineering & System Safety*, 140, 88-98.

[5] Nakajo, A., Mueller, F., Brouwer, J., Favrat, D. (2012). Progressive activation of degradation processes in solid oxide fuel cells stacks: Part I: Lifetime extension by optimisation of the operating conditions. *Journal of Power Sources*, 216, 449-463.

[6] Zaccaria, V., Tucker, D., Traverso, A. (2016). A distributed real-time model of degradation in a solid oxide fuel cell, part I: Model characterization. *Journal of Power Sources*, 311, 175-181.

[7] Zaccaria, V., Tucker, D., Traverso, A. (2016). A distributed real-time model of degradation in a solid oxide fuel cell, part II: Analysis of fuel cell performance and potential failures. *Journal of Power Sources*, 327 (2016) 736-742.

[8] Yan, D., Liang, L., Yang, J., Zhang, T., Pu, J., Chi, B., & Li, J. (2017). Performance degradation and analysis of 10-cell anode-supported SOFC stack with external manifold structure. *Energy*, 125, 663-670.

[9] Offer, G. J., & Brandon, N. P. (2009). The effect of current density and temperature on the degradation of nickel cermet electrodes by carbon monoxide in solid oxide fuel cells. *Chemical Engineering Science*, 64(10), 2291-2300.

[10] De Haart, L. G. J., Mougin, J., Posdziech, O., Kiviaho, J., Menzler, N. H. (2009). Stack Degradation in Dependence of Operation Parameters; the Real-SOFC Sensitivity Analysis. *Fuel Cells*, 9(6), 794-804.

[11] Petrone, R., Zheng, Z., Hissel, D., Péra, M. C., Pianese, C., Sorrentino, M., Yousfi-Steiner, N. (2013). A review on model-based diagnosis methodologies for PEMFCs. International *Journal of Hydrogen Energy*, 38(17), 7077-7091.

[12] Yuan, X. Z. R., Song, C., Wang, H., Zhang, J. (2009). *Electrochemical impedance spectroscopy in PEM fuel cells: fundamentals and applications*. Springer Science & Business Media.

[13] Pahon, E., Oukhellou, L., Harel, F., Jemei, S., & Hissel, D. (2014, May). Fault Diagnosis and Identification of Proton Exchange Membrane Fuel Cell System Using Electrochemical Impedance Spectroscopy Classification. *In Electrimacs*, 2014 (pp. pp-646).

[14] Tang, Y., Zhang, J., Song, C., Liu, H., Zhang, J., Wang, H., ... & Kozak, P. (2006). Temperature dependent performance and in situ AC impedance of high-temperature PEM fuel cells using the Nafion-112 membrane. *Journal of the Electrochemical Society*, 153(11), A2036-A2043.

[15] Huang, Q. A., Hui, R., Wang, B., Zhang, J. (2007). A review of AC impedance modeling and validation in SOFC diagnosis. *Electrochimica Acta*, 52(28), 8144-8164.
[16] Nechache, A., Cassir, M., & Ringuedé, A. (2014). Solid oxide electrolysis cell analysis by means of electrochemical impedance spectroscopy: a review. *Journal of Power Sources*, 258, 164-181.
[17] Nechache, A., Mansuy, A., Petitjean, M., Mougin, J., Mauvy, F., Boukamp, B. A. & Ringuedé, A. (2016). Diagnosis of a cathode-supported solid oxide electrolysis cell by electrochemical impedance spectroscopy. *Electrochimica Acta*, 210, 596-605.
[18] Changjun, X., & Shuhai, Q. (2011). Drawing impedance spectroscopy for Fuel Cell by EIS. *Procedia Environmental Sciences*, 11, 589-596.
[19] Yuan, X., Sun, J. C., Wang, H., & Zhang, J. (2006). AC impedance diagnosis of a 500W PEM fuel cell stack: part II: individual cell impedance. *Journal of Power Sources*, 161(2), 929-937.
[20] Wagner, N., & Gülzow, E. (2004). Change of electrochemical impedance spectra (EIS) with time during CO-poisoning of the Pt-anode in a membrane fuel cell. Journal of Power Sources, 127(1), 341-347
[21] Khan, S., Rizvi, S. A., Urooj, S. (2016, March). Equivalent circuit modelling using electrochemical impedance spectroscopy for different materials of SOFC. *In Computing for Sustainable Global Development (INDIACom)*, 2016 3rd International Conference on (pp. 1563-1567). IEEE.
[22] Hissel, D., & Pera, M. C. (2016). Diagnostic & health management of fuel cell systems: Issues and solutions. *Annual Reviews in Control*, 42, 201-211.
[23] Barelli, L., Barluzzi, E., & Bidini, G. (2013). Diagnosis methodology and technique for solid oxide fuel cells: a review. *International Journal of Hydrogen Energy*, 38(12), 5060-5074.
[24] Lee, T. H., Park, K. Y., Kim, J. T., Seo, Y., Kim, K. B., Song, S. J., ... & Park, J. Y. (2015). Degradation analysis of anode-supported intermediate temperature-solid oxide fuel cells under various failure modes. *Journal of Power Sources*, 276, 120-132.
[25] Hofmann, P., Panopoulos, K. D. (2010). Detailed dynamic solid oxide fuel cell modeling for electrochemical impedance spectra simulation. *Journal of power sources*, 195(16), 5320-5339.
[26] Zhu, H., Kromp, A., Leonide, A., Ivers-Tiffée, E., Deutschmann, O., & Kee, R. J. (2012). A model-based interpretation of the influence of anode surface chemistry on solid oxide fuel cell electrochemical impedance spectra. *Journal of The Electrochemical Society*, 159(7), 255-266.
[27] Fadaei, M., Mohammadi, R. (2015). A comprehensive simulation of gas concentration impedance for solid oxide fuel cell anodes. *Energy Conversion and Management*, 106, 93-100.
[28] Lang, M., Auer, C, Eismann, A., Szabo, P., & Wagner, N. (2008). Investigation of solid oxide fuel cell short stacks for mobile applications by electrochemical impedance spectroscopy. *Electrochimica Acta*, 53(25), 7509-7513.
[29] Montinaro, D., Contino, A. R., Dellai, A., & Rolland, M. (2014). Determination of the impedance contributions in anode supported solid oxide fuel cells with (La, Sr)(Co, Fe) O 3− δ cathode. *International Journal of Hydrogen Energy*, 39(36), 21638-21646.
[30] Zheng, Z., Petrone, R., Péra, M. C., Hissel, D., Becherif, M., Pianese, C., ... & Sorrentino, M. (2013). A review on non-model based diagnosis methodologies for PEM fuel cell stacks and systems. *International Journal of Hydrogen Energy*, 38(21), 8914-8926.
[31] Ding, S. (2008). Model-based fault diagnosis techniques: design schemes, algorithms, and tools. *Springer Science & Business Media*.
[32] Polverino, P., Pianese, C., Sorrentino, M., & Marra, D. (2015). Model-based development of a fault signature matrix to improve solid oxide fuel cell systems on-site diagnosis. *Journal of Power Sources*, 280, 320-338.

[33] Rosich, A., Sarrate, R., & Nejjari, F. (2014). On-line model-based fault detection and isolation for PEM fuel cell stack systems. *Applied Mathematical Modelling*, 38(11), 2744-2757.
[34] Buchholz, M., Eswein, M., & Krebs, V. (2008, September). Modelling PEM fuel cell stacks for FDI using linear subspace identification. *In Control Applications*, 2008. CCA 2008. IEEE International Conference on (pp. 341-346). IEEE.
[35] Steiner, N. Y., Candusso, D., Hissel, D., & Moçoteguy, P. (2010). Model-based diagnosis for proton exchange membrane fuel cells. *Mathematics and Computers in Simulation*, 81(2), 158-170.
[36] Wasterlain, S., Candusso, D., Harel, F., François, X., & Hissel, D. (2010, September). Diagnosis of a fuel cell stack using electrochemical impedance spectroscopy and bayesian networks. *In Vehicle Power and Propulsion Conference* (VPPC), 2010 IEEE (pp. 1-6). IEEE.
[37] Li, Z., Outbib, R., Giurgea, S., & Hissel, D. (2015). Diagnosis for PEMFC systems: a data-driven approach with the capabilities of online adaptation and novel fault detection. *IEEE Transactions on Industrial Electronics*, 62(8), 5164-5174.
[38] Chen, J., & Zhou, B. (2008). Diagnosis of PEM fuel cell stack dynamic behaviors. *Journal of Power Sources*, 177(1), 83-95.
[39] Steiner, N. Y., Hissel, D., Moçotéguy, P., & Candusso, D. (2011). Non intrusive diagnosis of polymer electrolyte fuel cells by wavelet packet transform. I*nternational Journal of Hydrogen Energy*, 36(1), 740-746.
[40] Damour, C., Benne, M., Grondin-Perez, B., Bessafi, M., Hissel, D., & Chabriat, J. P. (2015). Polymer electrolyte membrane fuel cell fault diagnosis based on empirical mode decomposition. *Journal of Power Sources*, 299, 596-603.

1.2. Monitoring algorithms implemented in commercial SOFC applications

AVL, Stefan Pofahl

As the manufactures do not disclose the inside of their operating strategies it is difficult to report on the state-of-the-art monitoring methods inside commercial SOFC systems. Nevertheless, patents disclose part of the current state of commercial systems internals. Therefore, AVLs literature survey focuses on patents and patent applications. Patents that focus on monitoring algorithms for a specific type of electrochemical reactors, specifically SOFC, are rare. If a specific type of fuel cell is mentioned, it is most of the time PEM fuel cells, this is even the case, if PEM is not mentioned in the title of the patent [5]. The patents can be split into monitoring methods/approaches [8] and monitoring hardware [6]. In some cases, methods and hardware are combined in patents [1]. In this section, the focus lies on patents that deal with methods rather than hardware.

1.1.5. Fuel and Media Monitoring

Toyota claims to be able to estimate the H2 concentration by evaluating the difference between expected and measured value of the impedance [3]. As the car manufacturer Toyota is not engaged in SOFC, it is unrealistic this method is implemented in SOFC systems. AVL holds patents as well that enable the estimation of media concentration in fuel cells. The first patent [11] protects the THDA methodology and is not limited to PEM fuel cells nor to fuel cells. Harting reported in [2] that the status of batteries can be monitored by means of nonlinear response analysis (NLRA), which is a different word for THDA. The most recent published patent [1] protect the hardware design for the current stimulus generation as implemented in the laboratory device THDA and the utilization of the principal of formation of intermodular responses to bi-chromatic excitation, c.f. chap. 1.1.31, this technique is also referred to as intermodular distortion analysis (IDA). Both patents are not yet implemented in SOFC systems. The patent by Jeong from Hyundai motor company [4] describes the hardware of a perturbation unit but describes at the same time a method for determination media shortage; the figure shown in the patent application is nearly identical to the one shown for the first time by Erich Ramschak [11], cf. Figure 5. A second patent from Hyundai [9] uses the term THDA which is claimed in for of a patent by AVL, again no reference can be found to [11], this patent focus on the type of excitation patterns.

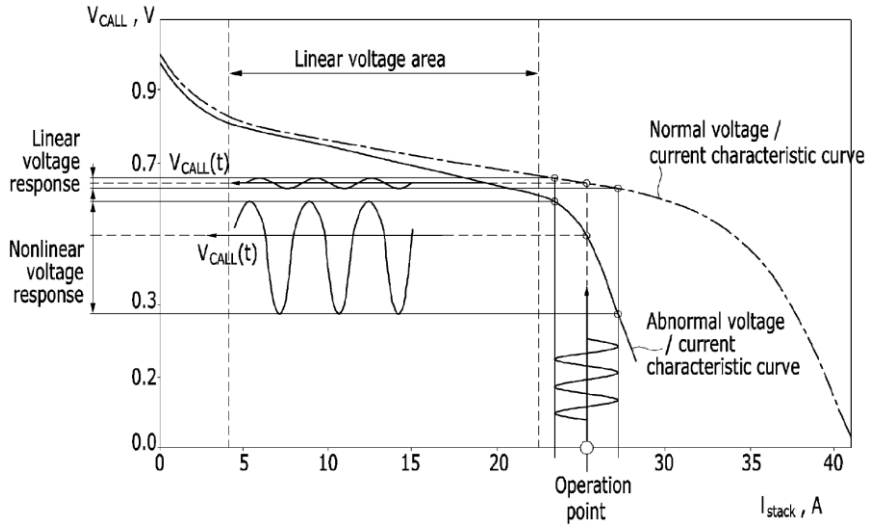

Figure 5: Principle of THDA depicted in [4] without reference to Ramschak [11].

1.1.6. State of Health Monitoring

Phlippoteau et.all. [10] gives his definition of State of Health as: *"state of health of the cell is estimated as the deviation between the estimated value of the parameter(s) with a predetermined reference value with the same parameter(s)"*. The patent covers all electrochemical reactors but focus

on PEM-fuel cell technology, as the company Helion[1], Aix (FR) which filed the patent was engaged only in PEM technology. It becomes not clear if the method can estimate the remaining usable life time of PEM-stacks, which is another definition of SoH. The patent describes different excitation techniques as multichromatic excitation.

1.1.7. Conclusion

The patents filed, dealing with stack monitoring, are manly filled from companies who deal with PEM fuel cell technology. Due to the cost of holding patents, most patents belong to companies in the automotive sector. From industry knowledge and the patents filled, it seems that stack monitoring by means of electrical AC-stimulation is not yet in use for SOFC technology.

1.1.8. Bibliography (Patents)

[1] Bernd Eichberger, Viktor Haker, Stephan Weinberger, Verfahren zum Überwachen des Betriebszustands von Brennstoffzellen, EP15181417, 2015

[2] Nina Harting, Nicolas Wolff, Fridolin Röder, Ulrike Krewer, Nonlinear Frequency Response Analysis (NFRA) of Lithium-Ion Batteries, Electrochimica Acta 248, p. 133–139, 2017

[3] Kotaro Ikeda, Tohiaki Kusakari, Hideaki Kume and others, Fuel Cell Hydrogen Concentration Estimation Device and Fuel Cell System, EP2429021A1, 2009

[4] K.S. Jeong, Y.B. Kum, S.H. Kim, H. Ko, Y.H. Lee, U.S. Kim, H. Park, Apparatus for diagnosing fault of fuel cell stack, US Patent 9,425,472, 2016

[5] Peter Kurzweil, Verfahren und Vorrichtung zur Überwachung des Betriebszustands einer elektrochemischen Vorrichtung, DE10220172A1, 2002

[6] Sebastian Lienkamp, Verfahren zum Messen eines Hochfrequenzwiderstandes einer Brennstoffzelle in einem Fahrzeug, DE102008046926A1, 2007

[7] R.R. Mosbæk, J. Hjelm, P.V. Hendriksen, R.G. Barfod, Solid Oxide Fuel Cell Stack Diagnostics, (Part of a PhD Thesis), Department of Energy Conversion and Storage, Technical University of Denmark, 2014

[8] Hyun-Seok Park, Anyang Uck-Soo, Sun-Doo Kang, Verfahren zum Überwachen eines Brennstoffzellenstapelstatus, DE102013114357A1

[9] Park, H. and Kim, U.S. and KANG, S.D., Method for diagnosing fault of fuel cell stack, US Patent 9,461,321, 2016

[10] V. Phlippoteau, A. Rakotondrainibe, C. Turpin, G. Fontes, Method for determining a state of health for an electrochemical device, US Patent 8,907,675, 2014

[11] Erich Ramschak, Method for monitoring the operational state of a fuel cell stack, US20060078788A1, 2004

[1] Helion have been taken over by Areva (FR).

1.3. Detection of Fuel Starvation

HTceramix, Jan-Pieter Ouweltjes

To benefit from the high efficiency of SOFC systems, its fuel cell stacks need to be operated with high fuel utilization, typically 80% or more. Employment of such high fuel utilizations brings along a potential risk where in extreme cases the fuel cells are prone to detrimental failure due to fuel starvation. Fuel starvation could, for example, be the result of sudden failure of the sealant while the stack is operated at high fuel utilization, or can occur during system transients, if fuel is consumed faster than it can be supplied by the fuel processing and delivery system [Gaynor, 2008]. Hence, operation at high fuel utilization should be done with care, with adequate control and mitigation strategies.

With respect to fuel cell monitoring, electrochemical impedance spectroscopy has shown to be a powerful tool. The basic idea of using electrochemical impedance spectroscopy to determine the fuel distribution in SOFC stacks was presented by Dekker et al. [Dekker, 2009]. Later, Mosbæk et al. have shown the correlation of low frequency responses to changes in gas supply over individual cells in stacks [Mosbæk, 2014]. Recently, Tallgren et al. have further refined the methodology by extending it also to cover temperature distributions within the stack [Tallgren, 2017].

Depending on the fuel utilization degree, the impedance response is progressively affected. Up to 80% fuel utilization, issues with fuel distribution will be reflected in the gas conversion impedance, which is typically observed at ≤ 1 Hz in the impedance spectra. Under more severe conditions, other features in the impedance spectra at frequencies above 1 Hz will also be affected. Das, for example, showed that upon increasing the fuel utilization from 70 to 90%, not only the gas conversion impedance increased, but also the bulk transport resistance (3 Hz) and the charge transfer resistance (630 Hz), be it to a lesser extent [Das, 2015]. In severe cases, fuel starvation will be observed, where the nominal oxygen partial pressure can be very close to the Ni oxidation potential, which can lead to re-oxidation of the anode catalyst (nickel), which could then result in irreversible loss in performance [Fang, 2015; Brus, 2015]. Lee et al. showed that such severe conditions could even trigger irreversible degradation at the cathode side, where it was speculated that cathode delamination occurred due to anode volume changes as a result of nickel re-oxidation [Lee, 2015].

It is clear that such severe conditions that lead to irreversible damage should be prevented in order to improve the lifetime of the SOFC stack. This is why many research groups are currently developing control strategies, monitoring routines and control hardware to keep stacks within safe operating boundaries. One option which rapidly gains interest, is Total Harmonic Distortion (THD). In such case the operating current is superimposed by an AC current signal with a specific frequency pattern (e.g. a sinusoidal pattern or a pseudo-random binary sequence) in order to trigger early warning signals before the stack experiences irreversible damage. Mosbæk et al., in a joint effort between DTU and AVL, were one of the first to successfully employ THD for SOFC stacks to detect fuel starvation, after the technique had previously been demonstrated for PEMFC stacks [Mosbæk, 2014]. THD has been further developed within the European project DIAMOND, and currently in the project INSIGHT. Recently, as an alternative to THD, it has been proposed to employ the Wavelet Transform (WT) technique for stack monitoring. While diagnostic tools developed with EIS methodology are model based (e.g. Equivalent Circuit Modeling) approaches, tools developed with WT are purely signal-based approaches. This means that the parameters used for the diagnostics with WT are directly extracted from the signal analysis with no need for a model [Esposito, 2016]. Though still in its infancy, WT has shown its potential, and has deserved its place as a potential monitoring tool to improve the stack lifetime.

1.1.9. Bibliography

[Gaynor, 2008] R. Gaynor, F. Mueller, F. Jabbari, J. Brouwer, On Control Concepts to Prevent Fuel Starvation in Soldi Oxide Fuel Cells, Journal of Power Sources 180 (2008) 330-342

[Fang, 2015] Q. Fang, L. Blum, R. Peters, M. Peksen, P. Batfalsky, D. Stolten, SOFC Stack Performance under High Fuel Utilzation, International Journal of Hydrogen Energy 40 (2015) 1128-1136

[Dekker, 2009] N.J.J. Dekker, J.F. van Wees, G. Rietveld,. Determination of the Anode Flow Distribution in a SOFC Stack at Nominal Operating Conditions by EIS, The Electrochemical Society, Vol. 25 no. 2 pp. 1871-1878, 2009

[Mosbæk, 2014] R.R. Mosbæk, J. Hjelm, P.V. Henriksen, R. Gottrup, Solid Oxide Fuel Cell Stack Diagnostics, Technical University of Denmark, 2014

[Tallgren, 2017] J. Tallgren, C. Boigues Munoz, J. Mikkola, O Himanen, J. Kiviaho, Determination of Temperature and Fuel Utilization Distributions in SOFC Stacks with EIS, ECS Transactions, The Electrochemical Society, vol.78 (2017) No.1 pp. 2141-2150

[Das, 2015] D. Das, Electrochemical Degradation, Kinetics & Performance Studies of Solid Oxide Fuel Cells, Dissertation, The Pennsylvania State University, Department of Energy & Mineral Engineering, 2015

[Fang, 2015] Q. Fang, L. Blum, R. Peters, D. Stolten, SOFC Stack Performance under High Fuel Utilization, International Journal of Hydrogen Energy 40 (2015) 1128-1136

[Brus, 2015] G. Bus, K. Miyoshi, H. Iwai, M. Saito, H. Yoshida, Change of an Anode's Microstructure Morphology during the Fuel Starvation of an Anode-Supported Solid Oxide Fuel Cell, International Journal of Hydrogen Energy, Vol. 40, Issue 21, 2015, pp. 6927-6934

[Lee, 2015] T.-H. Lee, K.-Y. Park, J.-T. Kim, Y. Seo, K.B. Kim, S.-J. Song, B. Park, J.-Y. Park, Degradation Analysis of Anode-Supported Intermediate Temperature Solid Oxide Fuel Cell under Various Failure Modes, Journal of Power Sources 276 (2015) 120-132

[Esposito, 2016] A. Esposito, L. Russo, C. Kaendler, C. Pianese, B. Ludwig, N.Y. Steiner, High Fuel Utilization in Solid Oxide fuel Cells: Experimental Characterization and Data Analysis with Continuous Wavelet Transform, Journal of Power Sources 317 (2016) 159-168

1.4. THD study on SOFCs

CEA, Bertrand Morel

There are only few references on THD study applied for fuel cells: PEMFC [1-3], methanol fuel cell [4] and only 3 references for SOFC: [1, 5-7].

Concerning THD study on SOFCs, Ramschak et al. [1] performed in 2006 THDA tests under stationary load conditions with a 50-cell SOFC stack. A small amplitude sinusoidal AC current signal (1% of the DC load) was superimposed to the system current. Air utilization (AU) values were increased by reducing air flowrate until the first cell voltage started to drop to a critical level of about 0.7 V. The THDA signal measured from the total stack voltage only can be used in an external control unit to decide about critical operation of the stack if e.g. a THDA-level of 4 is exceeded. Ramschak gives complementary information about the specifications of the THD device. The definition of the maximum number of cells in a stack, which can be monitored with the THDA technology, depends on one hand on the capability to separate large from relatively small and narrow spectral components and, on the other hand, on the stack (impedance) characteristics itself. Thus, specifications like resolution of the analogue–digital converter, sample frequency, window length settings for the frequency transformation, required time resolution for the output and stack impedance curve characteristics are the constraints for the calibration process of THDA.

THD experiments have been performed also by Mosbæk [5-6] on a 14-cell SOFC stack varying frequencies and amplitude of the AC signal and Fuel Utilization (FU). It was shown that THD can be used to detect increasing non-linearities in the i-V characteristics of the stack when the stack suffers from fuel starvation by measuring only the stack sum voltage. Mosbæk mentions also that the AC superimposed signal must be lower than 3 Hz in order to detect fuel starvation for this stack technology; by decreasing the AC signal frequency under 3 Hz and by increasing the AC amplitude, the THD value becomes higher, hence more sensitive to fuel starvation.

THD experiments have been performed by Morel et al. [7] on small size cell and also on a 6-cell SOFC stack from SOLIDpower varying frequencies (from 10 mHz to 10 kHz) and amplitude of the AC signal (1%, 5%, 10% and 20% of the DC signal), AU and FU. It appears that THD index becomes significant in the range of frequency between 1 and 0.01 Hz. This non-linear behavior in this range of frequency is not surprising because of mass transport issue which is a slow process. Hence, high FU can be detected with a high sensitivity at 10^{-2} Hz. AC excitation of only 1% of the DC current is not sufficient to get relevant THD index. It is preferable to use an AC signal with an amplitude of at least 5% of the DC signal.

1.1.10. Bibliography

[1] Ramschak, E., Peinecke, V., Prenninger, P., Schaffer, T., Hacker, V., 2006. Detection of fuel cell critical status by stack voltage analysis. Journal of Power Sources 157, 837–840. doi:10.1016/j.jpowsour.2006.01.009

[2] Thomas, S., Lee, S.C., Sahu, A.K., Park, S., 2014. Online health monitoring of a fuel cell using total harmonic distortion analysis. International Journal of Hydrogen Energy 39, 4558–4565. doi:10.1016/j.ijhydene.2013.12.180

[3] Mao, Q., Krewer, U., 2013. Total harmonic distortion analysis of oxygen reduction reaction in proton exchange membrane fuel cells. Electrochimica Acta 103, 188–198. doi:10.1016/j.electacta.2013.03.194

[4] Mao, Q., Krewer, U., Hanke-Rauschenbach, R., 2010. Total harmonic distortion analysis for direct methanol fuel cell anode. Electrochemistry Communications 12, 1517–1519. doi:10.1016/j.elecom.2010.08.022

[5] Mosbæk, R.R., Hjelm, J., Barfod, R., Høgh, J., Hendriksen, P.V., 2013. Electrochemical Characterization and Degradation Analysis of Large SOFC Stacks by Impedance Spectroscopy. Fuel Cells 13, 605–611. doi:10.1002/fuce.201200175

[6] Mosbæk, R.R., 2014. Solid Oxide Fuel Cell Stack Diagnostics. DTU, Ph.D. Thesis.
[7] Evaluation of Total Harmonic Distortion tool for SOFC diagnostics, Bertrand Morel, André Chatroux, Presentation during the "European Fuel Cell Conference & Exhibition" in Naples (Italy) in the FC Diamond workshop "Monitoring, Diagnostics and Control for SOFC systems", http://www.diamond-sofc-project.eu, 2016

1.5. EIS on SOFC: Carbon Deposition

AVL, Stefan Pofahl

The separation of different failure modes by means of EIS is difficult. Subotić states in [11]:
"*Altogether, a detailed electrochemical analysis of the cell behavior and sample early identification of adverse changes of the cell performance caused by wide variety of degradation mechanisms is missing in the literature and is essential for the further investigation of solid oxide fuel cells.*"
Carbon deposition in the anode compartment is specifically a topic for SOFC operated with carbon building fuels, as natural gas or diesel fuel, cf. [5], [6], [7], [8], [11] and [14].
As shown in [11], [4], [10], [12], [13] it is possible to detect carbon deposition by means of EIS in the low frequency range, but it is challenging to exclude other failure modes as a root cause for detected deviations in the impedance spectra of a stack under operation. To enhance the detectability of specific failure modes and to differentiate between anode and cathode the distribution of relaxation times (DRT) is a suitable method as presented e.g. in [2], [9] and [11]. In the early stage of carbon deposition, the performance of the SOFC might be enhanced as described in [3], [11]. The electrical conductivity of the anode is higher and the microporous electrode structure is not yet blocked by carbon. The reduced impedance in the low frequency domain as depicted in the Nyquist plot, cf. Figure 6 for the two curves 2, 3 might be related to changes in the fuel composition in the microporous electrode structure in contact with the TPB, as the low frequency domain refers to the gas conversion impedance. A comparison of the low frequency arc dependent on the fuel composition and current density is published in [11]. Two effects might lead to this result: a.) the thin carbon layer influences the species transport to the TPB dependent on the species, b.) part of the carbon might get re-oxidized, which leads to additional reactions.
Published results from THDA-tests are outstanding.

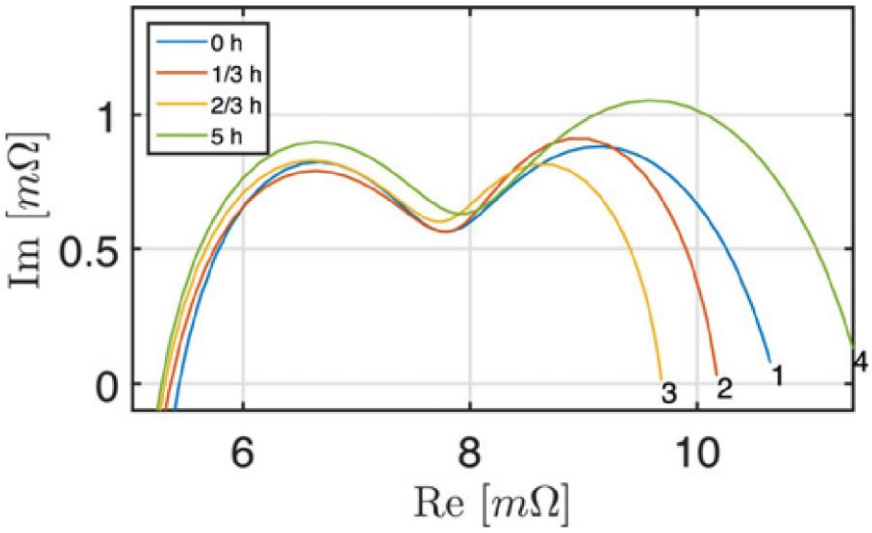

Figure 6: Influence of progressing carbon formation on the impedance in the low frequency domain[11]. With increasing thin porous carbon coverage of the anode, the impedance in the low frequency domain is decreasing (curves 1 – 3). After formation of a dense layer the impedance increases drastically (curve 4).

Remark:
If there is a steam reformer up-stream to the stack, carbon will be formed mainly in the reformer, therefore, there might be two alternative approaches to detect critical operation conditions that might favor carbon formation inside the stack: a.) energy balance around the steam reformer, b.) detection of fuel starvation (the reaction rate of the steam reforming process will slow down, if carbon is formed inside the reformer)

1.1.11. Bibliography

[1] K. Kendall, C. Finnerty, G. Saunders, J. Chung, Effects of dilution on methane entering an SOFC anode, Journal of Power Sources 106 (1-2) 323–327 p. 2002

[2] A. Kromp, A. Leonide, A. Weber, E. Ivers-Tiffée, Electrochemical Analysis of Reformate-Fuelled Anode Supported SOFC, J. Electrochem. Soc. 158 (8), p. B980–B986, 2011, http://jes.ecsdl.org/content/158/8/B980

[3] C. Mallon, K. Kendall, Sensitivity of nickel cermet anodes to reduction conditions, Journal of Power Sources 145 (2), p. 154–160, 2005

[4] J. Mermelstein, M. Millan, N. Brandon, The impact of carbon formation on Ni-YSZ anodes from biomass gasification model tars operating in dry conditions, Chemical Engineering Science 64 (3), p. 492–500, 2009.

[5] C.J. Moyer, N. P-Sullivan, H. Zhu, R.J. Kee, Polarization Characteristics and Chemistry in Reversible Tubular Solid-Oxide Cells Operating on Mixtures of H2, CO, H2O, and CO2, Journal of The Electrochemical Society 158 (2) p. B117–B131, 2011

[6] M. Pillai, Y. Lin, H. Zhu, R.J. Kee, S.A. Barnett, Stability and coking of direct-methane solid oxide fuel cells: Effect of CO2 and air additions, Journal of Power Sources 195, p. 271–279 2010

[7] C. Schluckner, V. Subotić, V. Lawlor, C. Hochenauer, Three-dimensional numerical and experimental investigation of an industrial-sized SOFC fueled by diesel reformate -Part II: Detailed reforming chemistry and carbon deposition analysis, Journal of fuel cell science and technology 12 (5) p.1-12, 2015

[8] G. Saunders, J. Preece, K. Kendall, Formulating liquid hydrocarbon fuels for SOFCs, Journal of Power Sources 131 (1-2) p. 23–26, 2004

[9] V.Sonn, A.Leonide, E.Ivers-Tiffée, Combined Deconvolution and CNLS Fitting Approach Applied on the Impedance Response of Technical Ni8YSZCermet Electrodes, J. Electrochem. Soc.155(7), B675–B679, 2008.

[10] V. Subotić, C. Schluckner, M. Joerg, J. Rechberger, H. Schroettner, C. Hochenauer, Anode regeneration following carbon depositions in an industrial-sized anode supported solid oxide fuel cell operating on synthetic diesel reformate, Journal of Power Sources 295 (0), p. 55–66, 2015.

[11] Vanja Subotić, Christoph Schluckner, Johannes Strasser, Vincent Lawlor, Jörg Mathé, Jürgen Rechberger, Hartmuth Schroettner, Christoph Hochenauer; In-situ electrochemical characterization methods for industrial-sized planar solid oxide fuel cells Part I: Methodology, qualification and detection of carbon deposition; Electrochimica Acta, 207, p. 224 – 236, 2016

[12] V. Subotic, C. Schluckner, H. Schroettner, C. Hochenauer, Analysis of possibilities for carbon removal from porous anode of solid oxide fuel cells after different failure modes, Journal of Power Sources 302, p. 378–386, 2016, http://www.sciencedirect.com/science/article/pii/S0378775315304584

[13] H. Sumi, K. Ukai, Y. Mizutani, H. Mori, C.-J. Wen, H. Takahashi, O. Yamamoto, Performance of nickel-scandia-stabilized zirconia cermet anodes for SOFCs in 3H2O-CH4, Solid State Ionics 174 (1-4), p. 151–156, 2004

[14] K.M. Walters, A.M. Dean, H. Zhu, R.J. Kee, Homogeneous kinetics and equilibrium predictions of coking propensity in the anode channels of direct oxidation solid-oxide fuel cells using dry natural gas, Journal of Power Sources 123, p.182–189 2003

1.6. EIS on SOFC: Anode Poisoning

HTceramix, Jan Pieter Ouweltjes

Early attempts to describe the electrochemical behavior of SOFCs operated under internal reforming conditions in the time-domain were presented by Zhu and Kee [Zhu 2006]. Their model included multicomponent porous-media transport, elementary heterogeneous chemical reaction, ion conduction, and electrochemical charge transfer, based on physical conservation laws. The simulations have shown that internal-reforming chemistry affects the impedance spectra significantly. Compared to the electrochemical response in hydrogen, more arcs can be seen in the impedance plots under methane reforming, mainly caused by the multiple time scales associated with heterogeneous reforming chemistry due to complex interactions between diffusive and chemical processes within the anode. Because the scales overlap, authors did not succeed to unambiguously relate the arc shapes in the impedance response to individual physical processes.

Further evidence for the more complex nature of impedance spectra obtained under reformate conditions follows from a publication by Kromp et al. [Kromp 2013]. Their model, which focused on charge-transfer reactions and equations transport phenomena within the anode substrate (including an empirically determined Knudsen factor to effectively describe the diffusion of CO and CO2), revealed that substrate diffusion would appear as two Warburg-shaped arcs in the impedance spectra, one for hydrogen-steam at higher frequency and a second one for CO-CO2 at lower frequency). The water gas shift reaction, which is typically fast at SOFC operating conditions, was found to have notable influence on the size of the two arcs, resulting in lower impedance for the hydrogen-steam arc and higher impedance for the CO-CO2 arc compared to a simulation (for the sake of comparison) where WGS was not assumed to occur.

Weber et al. [Weber 2013] investigated the impact of sulfur on the H2 electrooxidation and water gas shift kinetics for two types of anode supported cells with 1 cm2 active area, employing different anode functional layers and anode substrates. The cells were characterized by CV measurements and EIS measurements performed at OCV. EIS data were analyzed by DRT and subsequent fitting to physically meaningful equivalent circuits. Measurements were performed under different fuel compositions allowing for revealing the contribution of WGS. It was observed that under 0.5 ppm H2S, the increase in polarization resistance is mainly attributed to processes P2A (200 Hz) and P3A (4000 Hz), describing the coupling of ionic conductivity in the 8YSZ matrix, the H2 electrooxidation at the triple phase boundaries of the gas diffusion in the anode functional layer [Leonide 2008]. Looking at the ASR values, while separating the ohmic losses from the polarization losses, it can be observed that poisoning is mainly related to a change in polarization resistance. After testing up to 15 ppm S, it was found that regeneration to the original performance was very difficult and took at least longer than 100 h, and with unlikely full recovery. A much faster partial recovery can be achieved by polarizing the cell. In the case of reformate, not only P2A and P3A but also features at lower frequency related to H2/H2O gas diffusion (10-20 Hz) and CO-CO2 gas diffusion coupled to the WGS reaction (1 Hz) changed. The change in these features is related to poisoning of the nickel surfaces in the anode resulting in a deactivation of the shift-catalyst. Thus, CO and CO2 are no longer involved in the reaction and act as an inert component in the gas mixture. Furthermore, a feature at around 20 mHz pops up, which is somehow scaling with the degradation rate, i.e. it temporary increases during the poisoning process. This process might be related to the transient behavior during the poisoning resulting in an artificial peak in the DRT. Comparing the temporal characteristics of the polarization resistance of two different anode supported cells, it could be shown that the accumulated H2S amount divided by the Ni surface area inside the anode substrate and anode functional layer determine the onset of the degradation.

Hagen et al. [Hagen 2013] have investigated the response of anode supported cells to sulfur poisoning both in hydrogen-steam and hydrogen-steam-CO mixture. The increase of the polarization resistance is much larger in the hydrogen-steam-CO fuel, i.e. less H2S can be added, which is in agreement with the cell voltage observations. It seems also that the serial resistance starts to be affected at the highest concentrations in the hydrogen-steam-CO fuel. There is a distinct difference how sulfur affects the polarization region on the different fuels. In the hydrogen-steam fuel, the addition of sulfur gave rise to the high frequency region around

1000 Hz, while the low frequency region was not affected. According to previous detailed electrochemical studies on this type of cells, the region around 1000 Hz is assigned to the anode processes. Same for the poisoning effect in hydrogen-steam-CO fuel. A significant behavior is observed in the low frequency region. Here, a remarkable increase is caused by the addition of sulfur. The low frequency region around 1 Hz is due to conversion/diffusion impedance. The observed increase is an indication of lack of fuel to the anode in the hydrogen-steam-CO fuel and thus obviously of the supply of hydrogen due to the poisoning of the WGS reaction. General trends are more or less the same for 850 and 750°C. In hydrogen-steam, up to 92 ppm H2S was tolerated, while in hydrogen-steam-CO already 8 ppm H2S caused a dramatic increase of the polarization resistance.

Hauch et al. [Hauch 2014] have performed sulfur poisoning tests on different cells with methane-steam-hydrogen fuel and found that the reversibility of the poisoning was dependent on the overpotential; at low overpotential full recovery took place while it was partly irreversible after operation at high overpotential. Upon start of H2S addition, frequency in the range 1-3 kHz increased significantly which is associated to the charge transfer reaction. Operation at high overpotential was also associated to an increase of the ohmic losses. Without H2S, operation at high overpotential was without problems, indicating that the degradation is due to the sulfur poisoning. Post mortem analysis revealed that the cell operated with S and high overpotential exhibited a significant lack of percolating Ni in the 2-4 micron closest to the electrolyte, whereas the percolating Ni network in the region further away from the anode/electrolyte interface seems unaltered. The loss in Ni percolation can be caused by different phenomena: 1) buildup of impurities between Ni particles, 2) nano-scale morphology changes 3) evaporation as Ni-hydroxide species, 4) diffusion of Ni. Even though it is clear from SEM images that the innermost few microns of the anode from the test under high polarization has a decreased Ni content, it has not been possible to locate and quantify the Ni elsewhere in the cell.

Montinaro et al. have performed a parametric study under both hydrogen and reformate, including the influence of sulphur. The results are a bit difficult to interpret due to the fact that the impedance measurements were performed under potentiostatic conditions. Under operation with methane-steam mixture, the gas conversion impedance (appearing at around 0.1 Hz) was found to exhibit parabolic behavior as function of the steam concentration, while the contribution at 1.5 kHz (charge transfer) was found to increase linearly with decreasing steam-to-carbon ratio. As the cell at some moments was operated at S/C ratios below unity, it was suspected that the latter could be related to carbon deposition. Sulphur poisoning was mainly reflected in the arc occurring at high frequency which was found to be related to the charge transfer reaction. [Montinaro 2014].

Madi et al. characterized anode supported cells under synthetic gas compositions simulating biogas or bio-syngas, including their typical impurities. It was found that organic sulphur when using bio-syngas mainly affected the polarization arc at a relaxation frequency of around 500 Hz, which was found to be related to the charge transfer reaction with linear dependency on the organic sulphur concentration, while the second arc at a lower frequency below 1 Hz, which was found to be related to gas conversion impedance, hardly changed. In one case, full recovery was observed after removing the contaminant, while in two other cases only partial recovery was observed [Madi 2016-1]. In another paper, the impact of HCl on the electrochemical performance was reported, and which was found to affect both the charge transfer reaction at high frequency and the gas conversion impedance at low frequency. Upon HCl removal, partial recovery was observed, but this mainly concerned the gas conversion impedance [Madi 2016-2]. Also, siloxanes were found to affect both the anode charge transfer reaction at high frequency and the gas conversion impedance at low frequency [Madi 2015].

Papurello et al. investigated the impact of H2S on the anode performance with hydrocarbon containing fuel and found that this had a considerable impact on the mass transport resistance appearing at low frequency [Papurello 2016-1]. Earlier, this group has shown that upon exposure to sulphur, the entire available Ni surface is affected by sulphur contamination and not just the TPB region, and that the sulphur coverage can be described well by the Temkin isotherm, as previously shown by Hansen [Papurello 2015, Hansen 2008]. It is

thus to be noted that this is different from observations in syngas from Madi et al, which implies that the reforming reaction is impeded by the presence of sulphur, after which methane merely acts as diluent. In another publication from Papurello et al., in which the impact of naphthalene has been reported, it was shown that this compound inhibits both the charge-transfer reaction and gas conversion impedance, where it is assumed that the nickel surface is no longer available for adsorption and desorption of gas compounds involved in the reforming of methane and the water-gas shift reaction [Papurello 2016-2].

Doyle et al. investigated the impact of toluene, and found that this mainly affected the gas diffusion process due to carbon deposition, and reflected in the impedance arc with a relaxation frequency below 1 Hz [Doyle 2014]. Zhi et al. investigated the effect of exposing Ni-YSZ anode to phosphine, and found that both the charge-transfer resistance and the diffusion resistance increased, the diffusion resistance increasing proportionally faster than the charge transfer resistance. Post mortem analysis revealed the formation of Zr and Ni phosphates which suppressed the electrocatalytic activity of the anode and were found to block the gas diffusion channels and disrupt charge transport pathways in the electrode [Zhi 2008].

1.1.12. Bibliography

[Zhu 2006] H. Zhu, R. Kee, Modeling E;lectrochemical Impedance Spectra in SOFC Button Cells witt Internal Methane Reforming, J.El.Soc. 153 (9) (2006) A1765

[Kromp 2013] A. Kromp, H. Geisler, A. Weber, E. Ivers-Tiffee, Electrochemical Impedance Modeling of Gas Transport and Reforming Kinetics in Reformate Fueled Solid Oxide Fuel Cell Anodes, Elec.Acta 106 (2013) 418-424

[Weber 2013] A. Weber, S. Dierickx, A. Kromp, E. Ivers-Tiffee, Sulfur Poisoning of Anode-Supported SOFCs under Reformate Operation, Fuel Cells 13, 2013, No. 4, 487-493

[Hagen 2013] A. Hagen, Sulfur Poisoning of the Water Gas Shift Reaction on Anode Supported Solid Oxide Fuel Cells, J. Electrochem. O.c 160 (20) F111-F118 (2013)

[Hauch 2014] A. Hauch, A. Hagen, J. Hjelm, T. Ramos, Sulfur Poisoning of SOFC Anodes: Effect of Overpotential on Long-Term Degradation, J. Electrochem. Soc. 161 (6) F734-F743 (2014)

[Montinaro 2014] D. Montinaro, A.R. Contino, A. Dellai, M. Rolland, Determination of the Impedance Contributions in Anode Supported Solid Oxide Fuel Cells with (La,Sr)(Co,Fe)O3-d Cathode, Int.J.Hydrogen Energy 39 (2014) 21638-21646

[Madi 2016-1] H. Madi, S. Diethelm, C. Ludwig, J. Van Herle, Organic-Sulfur Poisoning of Solid Oxide Fuel Cell Operated in Bio-Syngas, Int.J. Hydrogen Energy 41 (2016) 12231-12241

[Madi 2016-2] H. Madi, A. Lanzini, D. Papurello, S. Diethelm, C. Ludwig, M. Santarelli, Solid Oxide Fuel Cell Anode Degradation by the Effect of Hydrogen Chloride in Stack and Single Cell Environments, J. Power Sources 326 (2016) 349-356

[Madi 2015] H. Madi, S. Diethelm, S. Poitel, C. Ludwig, Damage of Siloxanes on Ni-YSZ Anode Supported SOFC Operated on Hydrogen and Bio-Syngas, Fuel Cells 15(5), 718-727, 2015

[Papurello 2016-1] D. Papurello, A. Lanzini, D. Drago, P. Leone, M. Santarelli, Limiting Factors for Planar Solid Oxide Fuel Cells under Different Trace Compound Concentrations, Energy 95 (2016) 67-78

[Papurello 2015] D. Papurello, A. Lanzini, S. Fiorilli, F. Smeacetto, R. Singh, M. Santarelli, Sulfur Poisoning in Ni-Anode Solid Oxide Fuel Cells (SOFCs), Chem. Eng. J. 283 (2015) 1224-1233

[Papurello 2016-2] D. Papurello, A. Lanzini, P. Leone, M. Santareli, The Effect of Heavy Tars (Toluene and Naphthalene) on the Electrochemical Performance of an Anode-Supported SOFC running on io-Syngas, Ren.En. 99 (2016) 747-753

[Hansen 2008] J.B. Hansen, Correlating Sulfur Poisoning of SOFC Nickel Anodes by a Temkin Isotherm, El.Sol.St.Lett. 2008 volume 11, issue 10, B178-B180 (2008)

[Doyle 2014] T.S. Doyle, Z. Dehouche, P.V. Aravind, M. Liu, S. Stankovic, Investigating the Impact and Reaction Pathway of Toluene on a SOFC running on Syngas, Int.J. Hydrogen Energy 39 (2014) 12083-12091

[Zhi 2008] M. Zhi, X. Chen, H. Finklea, I. Celik, N.Q. Wu, Electrochemical and Microstructural Analysis of Nickel-Yttria Stabilized Zirconia Electrode Operated in Phosphorous-Containing Syngas, J. Power Sources 183 (2008) 485-490

1.7. Electrochemical Impedance Spectroscopy of SOFC Cathode and Chromium poisoning

EPFL, Priscilla Caliandro, Arata Nakajo, Jan Van herle

1.1.13. Introduction

LSCF6428 is nowadays the most common material as cathode for Solid Oxide Fuel Cells. It is a single solid phase mixed ionic and electronic conductor (MIEC) with improved conductivities at intermediate temperature operation conditions (700°C), compared to materials used in previous generation cells, such as LSM-YSZ [1–3]. Because LSCF reacts with the standard YSZ electrolyte material to form an insulating secondary phase ($SrZrO_3$), a GDC interlayer is applied as buffer material between the electrode and the electrolyte to limit this effect [4]. The GDC has also been employed as scaffold for impregnation by LSCF, as a result, this composite cathode (LSCF-GDC) showed improved performances compared to the pure LSCF [5–7], due to the increased effective ionic conductivity resulting in an extension of the electrochemically active region.

Despite the good performances, questions remain about the stability of the material during very long-term operation. The main degradation for this material may stem from:

- Operating conditions leading to material destabilization:
  - Humidity
  - Temperature
  - Oxygen partial pressure
  - Polarization current
- Material composition alteration
  - Sr segregation
  - Co depletion
- Secondary phase formation from:
  - electrode/electrolyte interaction
  - MIC/electrode interaction
- Poisoning:
  - Cr
  - Si
  - S

These degradation mechanisms are reviewed based on the available literature for the two most widely studied cathode configurations (LSCF and LSCF-GDC).

1.1.14. Frequency range of cathodic processes

A screening of cathodic process degradation signs on single cell and single repeat unit is first presented to support further discussions about the degradation features on the EIS response reported in the literature.

KIT

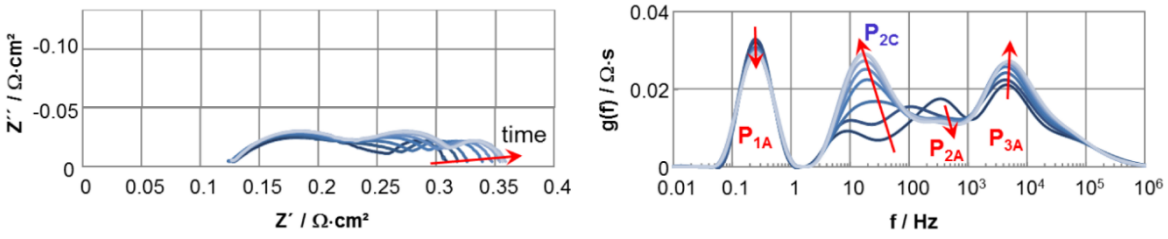

ASCs with Ni-YSZ anode substrate, Ni-YSZ AFL, YSZ electrolyte, GDC buffer layer and LSCF cathode. Impedance spectra of a single cell measured during a 1000 h test at 750°C under OCV conditions, 50%CO/50%CO_2 and Air [8]. Where P_{1A} is the resistance related to gas-phase diffusion at the anode, P_{2C} P_{2A} and P_{3A} are losses related to the activation polarization in the anode and cathode.

DTU

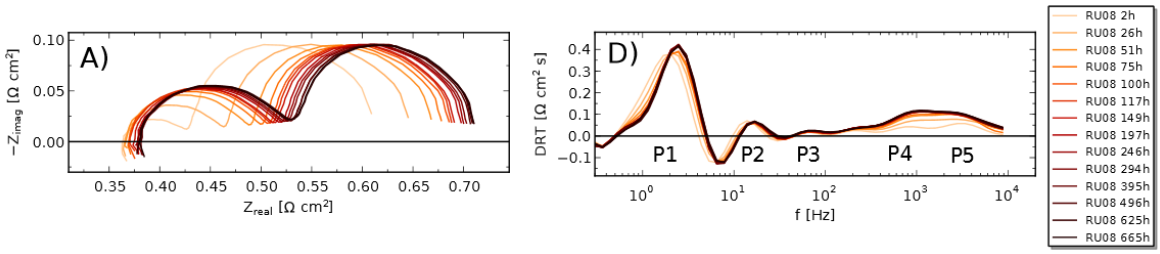

SRU from a planar 14 cell stack with Ni-YSZ supports, Ni-YSZ anodes, YSZ electrolytes, GDC buffer layer and LSCF-GDC composite cathodes (P3 is the activation polarization at the cathode 100 Hz to 1 kHz). Impedance spectra measured during a 665 h test at 700°C at 0.22 A/cm^2, 52% FU, 50%H_2/50%H_2O Air [9].

HTCeramix-SOLIDpower

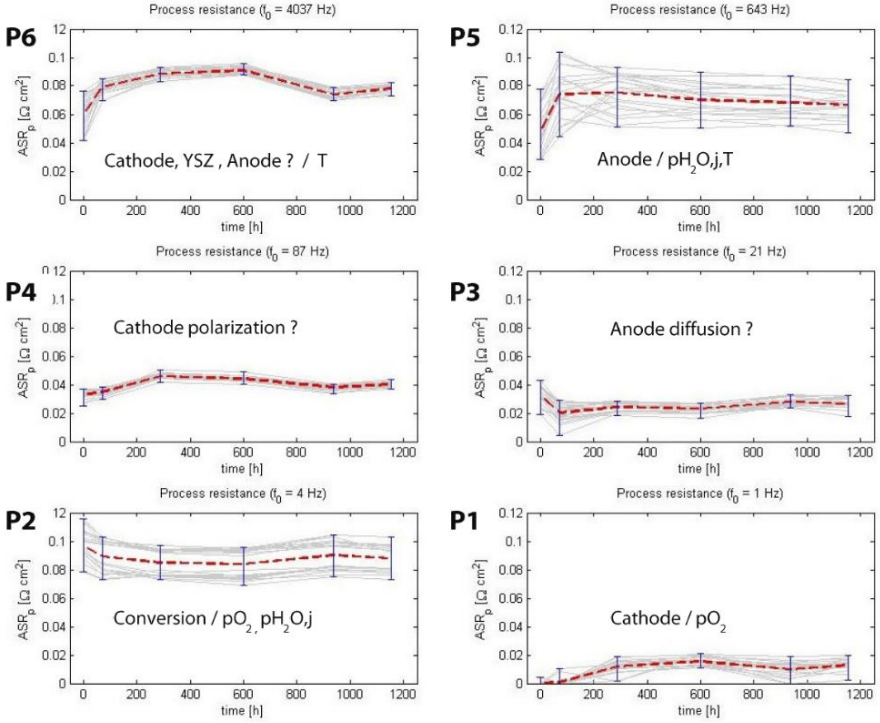

Segmented planar cell with Ni-YSZ anode support, Ni-YSZ anode, YSZ electrolyte, GDC buffer layer and LSCF cathodes (P4 is the activation polarization at the cathode 100 Hz). Impedance spectra of 20 segments measured during a 1200 h test at 700°C at 0.1 A/cm^2, 60%H_2/40%N_2-Air [10]

The cathode process frequency range is located in the frequency range around 100 Hz, with slight variations depending upon the cells configurations and supplier. Recently an impedance model of LSCF and LSCF-GDC cathodes was presented by Hubert et al. [11]. In this study, symmetrical cell impedance spectra were simulated with a physical based model and fitted with an equivalent circuit. The goal was the identification of regimes in the contributions of the surface and bulk reaction pathways depending upon polarization (cathodic/anodic) and microstructural properties. Characteristic frequencies of the spectra were estimated by sensitivity analysis for the single solid phase LSCF electrode: around 0.5-1 Hz for the surface reaction, around 5-100 Hz for bulk solid-state transport and up to 1 kHz when surface transport is involved and higher than 1000 Hz for charge

transfer reactions. The simulation results indicated that a composite LSCF-GDC is beneficial especially under anodic current condition, because the surface pathway dominates in this regime, whereas under cathodic polarization and OCV, the difference in performance is less.

1.1.15. Summary table

Discussion in section 4 below

Degradation Mechanisms		***LSCF***	***LSCF-GDC***
Operation condition	*pO2*	[3]	
	T	[3][12]	[13][6]
	current	[3]	
	Humidity	[14]	[13][15]
	CO2	[16]	[13]
Material composition alteration		[17][18]	
Second phase formation		[3][5]	
Poisoning	*Cr*	[19][20][21][22]	[23][24][25]
	Si	[26]	
	S	[27][28]	

1.1.16. LSCF

1.1.16.1. Operation Conditions

Contradictory results exist on the influence of operating conditions on long term degradation of a LSCF electrode under cathodic polarization.

For single solid phase LSCF, the influence of the operation conditions on long term degradation has been reported by Mai et al. [3]. Anode supported cells (Ni-YSZ/YSZ/GDC/LSCF) tested for 1000 h, at different temperature, oxygen partial pressure and polarization current, highlighted that ASR degradation proceeds faster at 800°C with respect to 700°C and with 21% of O_2 in the feed stream instead of 5%. A clear trend regarding the polarization current could not be revealed by this study. The reported evolution of the impedance spectra for the cell tested at 700°C shows performance degradation in the frequency range from 0.1 Hz to 1 kHz.

A different outcome concerning the temperature effect on long term degradation is reported by Endler-Schuck et al. [12]. The authors tested an ASC (Ni-YSZ/YSZ/GDC/LSCF) for 1000 h in an Al_2O_3 test bench recording EIS each 8 h under OCV and at three different temperatures: 600, 750, 900°C. Using the Distribution of Relaxation Times (DRT) technique they could discriminate the cathode process contributions (10 to 100Hz) from the total polarization resistance. The cathodic process degradation rate was highest for the test at 600°C (Rpol: 0.209%/h, Rcat: 0.734%/h). Much smaller degradation was observed during testing at 750 and 900°C. No post-mortem analysis is presented for these two tests but the formation of $SrZrO_3$ secondary phase between the buffer layer and the electrolyte or the decomposition of the cathode material are listed as potential reasons for the degradation.

The effect of air moisture on the degradation of LSCF was documented by Liu et al. [14] by testing for 1000 h an electrolyte supported cell ESC (Ni-ScSz/ScSZ/GDC/LSCF) at 800°C, polarized at 200 mA/cm^2, under dry and humidify air (3, 5, 10 and 20% steam partial pressure). The ohmic and polarization cathode resistance was measured using current interruption technique. The study showed that degradation increases with higher

vapor concentration and it becomes severe by lowering the temperature at fixed humidification level. The effect of temperature on long term degradation is attributed to microstructural alterations. For the tests conducted at 900°C and 800°C with 10% humidified air FESEM observations showed no qualitative change of microstructure while they pointed out reduced porosity for the test performed at 700°C for which the cathode side ohmic resistance increase is the main contribution to degradation. The effect of water vapor on long term degradation is attributed to cathode material compositional change and migration on the surface rather than electrode/electrolyte interaction. FESEM EDX analysis revealed the formation of SrO as well as Fe enrichment, after 1000 h test at 800°C with 5% humidified air, on the surface of LSCF.

EIS analysis of the degradation of LSCF cathode due to the presence of CO_2 in the cathode flow is not yet available, but has been studied by AFM-DFT for LSCF thin film [16]. In the study, the surface degradation of LSCF thin films deposited on $NdGaO_3$ substrates were investigated by total reflection X-ray fluorescence (TXRF). Two situations were compared: annealing at 800°C in high (30%) and free CO_2 partial pressure with constant oxygen partial pressure in both cases. The choice for the high pCO_2 value is justified in presence of leakage from the sealing or cell cracks; in this case the cathodic compartment may be exposed up to a concentration of CO_2 equal to 30%. The results showed that the presence of CO_2 enhances the kinetics of Sr segregation on the surface. It is believed that strontium carbonate ($SrCO_3$) is an effective intermediate for Sr segregation and thus SrO phase formation that results in a decrease of the electrode specific surface area and of the surface electrocatalytic properties for the ORR process. Thus, both ohmic and polarization resistance can be affected by presence of CO_2 in the air compartment.

1.1.16.2. Material composition alteration

Several studies indicate that LSCF may locally change its composition during operation, up to decomposition.

Compositional changes were studied by Hardly et al. [17] by in-situ XRD combined to EIS. Anode supported cell with a SDC buffer layer and LSCF (Ni-YSZ/YSZ/SCD/LSCF) fed by air and 3% humidified H_2 respectively at cathode and anode side was characterized for 60 h at 750°C. EIS were recorded under polarization corresponding to an operating voltage of 0.8V. The high frequency process was mainly responsible for the degradation. XRD measurements detected a lattice expansion of the LSCF phase by 0.00004Å per hour. SEM EDX analysis indicated the migration of Sr and Co from the cathode to the buffer layer.

Sr segregation is commonly mentioned as a main reason for the degradation in the literature, but the effect on the ORR was just recently studied by Wang et al. [18]. The authors tested symmetric cells with porous $La_{0.6}Sr_{0.4}Co_{0.2}Fe_{0.8}O_{3-\delta}$ (LSCF) cathode on $Gd_{0.1}Ce_{0.9}O_{1.95}$ (GDC) electrolytes exposed to 800°C for 800 h and ambient air without polarization. EIS measurements performed periodically at 700°C (typical operation temperature) at OCV with a perturbation voltage of 20 mV showed a continuous increase of the polarization resistance. Spectra could be fitted accurately with a modified Gerisher type element. FIB-SEM analysis did not show particular changes in the microstructural parameters but inductively coupled plasma-optical emission spectrometry (ICP-OES) highlighted the presence of a Sr-rich surface on the aged sample. From EIS and microstructural analysis the authors extracted input parameters for the ALS model and computed the oxygen surface exchange rate k_0 and solid-state oxygen diffusion coefficient D*. The aging effect caused a decrease of both parameters by approximately 50%, the first presumably explained by the increase in Sr surface and the second by Sr depletion in the sub-surface of LSCF.

1.1.16.3. Secondary phase formation

Because of the high reactivity between LSCF and YSZ, a GDC buffer layer is commonly applied to mitigate the formation of non-conductive phase formation (e.g. $SrZrO_3$). In fact, due to the high activity of Sr in LSCF, this element may diffuse through the pores of the buffer layer and reach the surface of the electrolyte. Thus the composition, morphology and thickness of the buffer layer influences the amount of formed $SrZrO_3$ [29].

$SrZrO_3$ formation is in general considered critical during cell fabrication, and potentially as one contribution among several for cell degradation in operation.

Constantin et al. [5] studied the effect of GDC layer thickness (0, 0.45, 0.2 μm) in air at 700°C for 280 h. The electrochemical characterization was carried out by EIS on two electrodes cell made by an electrolyte supported cell (YSZ) on which Pt paste and GDC/LSCF (4 μm) electrode were applied. For all the tested samples, the measurements highlighted that degradation is more related to the increased polarization resistance rather than ohmic resistance. This effect tends to decrease if the buffer layer thickness increases. The authors related the change in polarization resistance to the formation of $SrZrO_3$ insulating phase that limits the active region area.

1.1.16.4. Cathode poisoning (Cr, S, Si)

Sr segregation occurs already under high temperature without Cr and it reacts with O_2 present in the air forming SrO. However, Cr volatile species have higher activity than O_2, their presence is expected to cause increased degradation with respect to a Cr free atmosphere [30].

A recent and detailed analysis of Cr poisoning of LSCF was reported by Ni et al. [20]. Symmetrical cells with LSCF deposited on GDC electrolyte support were characterized by EIS and electron and ion microscopy. One cell was tested after impregnation by a Cr solution (by heat treatment at 900°C for 5 h) and the second one was kept as reference. EIS was recorded at different temperatures between 600°C to 900°C at OCV and with a perturbation signal of 100 mV. Degradation by Cr poisoning was attributed to the increase of ohmic and polarization resistance both at low and high frequency, which doubled compared to the free Cr sample. By fitting the spectra, the oxygen surface exchange coefficient k_0 and oxygen diffusion coefficient D were estimated with the ASL model. Degradation by Cr poisoning resulted in a degradation of both parameters, compared with the free Cr sample. The explanation provided for the performance decrease was linked especially to nanoscale modification. In fact, SEM analyses could not reveal particular microstructural changes in the two samples. In contrast, low intensity peaks were observed in the XRD measurements of the impregnated samples, corresponding to the monoclinic $SrCrO_4$ phase, which can lower the conductivity and the number of active sites for oxygen exchange as well as the oxygen vacancy concentration due to Sr depletion. The reduction of oxygen diffusion coefficient can be linked at nanoscale level, to the incorporation of Cr into LSCF, at the grain boundary, consistent with Co and Fe depletion.

Shen et al.[19] documented the effect of Cr poisoning with respect to air moisture in the cathode compartment feed. A three-layer sandwich made of YSZ/LSCF/AISI 441 was tested in dry and 3% humidified air for 100 h under 200mA/cm^2. Microstructural analyses of the region near the interface with the AISI 441 based on SEM revealed a larger and wider solid phase size distribution after thermal treatment in dry air, but smaller and narrower in humidified air. Electrochemical impedance spectra showed that ageing under dry air leads to higher ohmic and polarization losses with respect to humidified air, though, the initial conditions improved for the first (dry) and worsened for the second (wet). The activation/passivation process is mainly attributed to the low frequency polarization resistance. EDX measurements highlighted that humidified air causes a decrease of Fe (and Co) concentration, whereas that of Cr increases. Cr deposition at the cathode/electrolyte interface is consistent with Sr distribution, explaining the Sr segregation from the LSCF through the interaction with Cr. It has to be noted that no buffer layer was used for this experiment.

Cho et al. [21] studied the effect of polarization on the degradation due to Cr on two ESCs made by LSCF/GDC/Pt, one aged at OCV for 75 h and the other aged under polarization (corresponding to an operating voltage of -0.2 V at LSCF) for 280 h in 3% humidified air. Even if the detected concentration of Cr was higher in the sample aged under polarization than in that kept at OCV, the degradation of the polarization resistance was lower. This effect was attributed to the distribution of deposited Cr rather than the amount of deposited Cr, to which the LSCF seems more sensitive. Considering the two samples aged for 75 h, EDX/WDS observation revealed that at OCV Cr and Sr were located mainly at the pores inside the LSCF (suggesting $SrCrO_4$ formation), while for the polarized sample, Cr deposition was observed on the top surface of LSCF.

SEM observations highlighted a significant change in the microstructure of the samples operated under polarization, correlated to Sr transport to the top surface of the LSCF cathode layer. Considering the EIS analysis, Cr poisoning was responsible for the degradation of the low frequency processes, such as oxygen adsorption and dissociation reaction sites on the LSCF surface.

A different effect is documented in the study by Oh et al. [22]. Symmetrical cells (LSCF/GDC/LSCF) were tested and the measurement results suggested that Cr poisoning affects the high frequency region associated to surface reaction mechanisms. Degradation in the surface properties was further detected by temperature programmed isotopic exchange (TPX) analysis. The onset temperature (corresponding to a formation of $^{18}O^{16}O$ and $^{16}O_2$ from adsorbed $^{18}O_2$) increased in presence of chromium if compared to the same sample tested without Cr-source at the same operating temperature. SEM/EDX and XRD analysis revealed the formation of a catalytically inactive phase ($SrCrO_4$) in combination with a Sr deficient layer extended to the total electrode surface. The lower concentration of Sr is directly linked to lower concentration of oxygen vacancy or whole concentration and thus degradation of the electrical conductivity and catalytic activity of the metal oxide.

Not only Cr acts as poisoning agent for LSCF cathode material. Other investigated contaminants are S and Si.

Perz et al. [26] investigated the effect of Si on symmetrical LSCF/GDC/LSCF cells (respectively thickness of GDC and LSCF are 1.8 mm and 30 μm) fed by ambient air during 2400 h at 700°C by means of EIS and SEM/TEM analysis. For the first 1060 h the sample was aged in free Si atmosphere. Later, in order to simulate Si poisoning, the cell was cooled down, a 10nm Si layer was sputtered on both cathodes and it was heated up again for the remaining time (1340h). The effect of Si poisoning on impedance has been linked to a low frequency process: gas diffusion/oxygen surface adsorption passivation. STEM analyses indicated that the deactivation is caused by the phase decomposition of LSCF and the formation of a La-Sr-silicate layer. On top of this surface, $(Co,Fe)_xO_y$ nanoparticles were detected.

S poisoning of LSCF can occur because of small concentrations in compressed air. Wang et al. [27] investigated the degradation of LSCF/GDC/Pt cell aged for 24 h at different concentration of SO_2: 0.1, 1, 10, 100 ppm at 800°C under current equivalent to a voltage of -0.2 V to the cathode vs. the air reference electrode. EIS was combined with XRD, SEM and thermodynamic calculations. Three dominant degradation mechanisms depending on the concentration of contaminant were proposed. Performance losses became more important at increased SO_2 concentration, leading to an increase in both ohmic and polarization resistance with the larger contribution occurring at low frequencies. The explanation for this effect was related to the formation of $SrSO_4$ that starts at the grain surface and extends to the whole surface as SO_2 concentration reached 100 ppm. Because of the covered active region, the adsorption mechanism of oxygen atoms is compromised. The increased value of high frequency polarization and ohmic resistance is attributed to the precipitation of $CoFe_2O_4$, resulting in a material composition approaching $LaFeO_3$ (lower oxygen vacancy concentration) and to an increased ionic path in order to reach the still available active sites. When SO_2 concentration reached 100 ppm, also La in the perovskite structure starts reacting with SO_2 forming $La_2O_2SO_4$. The decrease in performance was however not catastrophic, suggesting possible recovery.

The effect of S species on LSCF cathode was studied by Liu et al. [28] on electrolyte supported cells (LSCF/GDC/ScSZ/Ni-ScSZ) tested with 3vol% humidified H_2 at the anode and SO_2-containing air (0.1, 1, 5, 20, 40 ppm) to the cathode. Cell voltage at a constant current density of 200 mA/cm^2 was measured at 800°C for 1000 h. During experiments, cathode-side IR loss and cathodic polarization were measured by the current interruption method. Results indicate that cathodic polarization and degradation rate increased with increasing SO_2 concentration. Segregated particles were observed by SEM after the test with 20 ppm SO_2, EDX analysis identified them as compounds of strontium and sulfur.

1.1.17. LSCF-GDC

1.1.17.1. Operating conditions

Material stability and ORR kinetics for a composite cathode LSCF-GDC (50% weight $La_{0.6}Sr_{0.4}Co_{0.2}Fe_{0.8}O_{3-\delta}$ - 50% weight $Gd_{0.1}Ce_{0.9}O_{1.95}$) under operating environment was studied by Pellegrinelli et al. [13]. LSCF-GDC/GDC/LSCF-GDC symmetrical cells were tested at 450 and 750°C, respectively for 350 and 500 h, in air with either 3% H_2O or 5% CO_2 by EIS. Low and high frequency arcs are considered related respectively to chemical reaction processes between oxygen gas and the cathode and to the interfacial resistance between LSCF/GDC. However, the aging test in 3% of H_2O showed no degradation for the test conducted at 450°C while a significant increase of the ohmic resistance occurred for the cell aged at 750°C (most probably due to temperature rather than to air humidity). The aging test in 5% of CO_2 showed increased low frequency arc for the cell operated at 450°C, this degradation was completely recovered after switching off the CO_2 supply. At 750°C, as for the case of 3%H_2O, the main degradation contribution is the increase in ohmic loss most likely due to sintering.

The absence of degradation on a long term test (1200 h 750°C at 0.41 A/cm^2) in presence of humidified air for a LSCF-GDC/GDC/YSZ/Ni-YSZ cell was also reported by Nielsen et al. [15].

Effect of different temperatures, 650-700-800-850°C, on the composite cathode was studied by Shah et al. [6] on symmetrical LSCF-GDC/GDC/LSCF-GDC cell aged for 600 h in air with no current applied. EIS analysis highlighted higher degradation of the polarization resistance at higher temperature. Considering the spectra at 850°C a frequency shifts of the maximum of the Bode plot from 100 Hz to 10 Hz was recorded. No big changes in microstructure were noted for the aged sample at 600°C while substantial decrease of LSCF surface area for the sample aged at 850°C was observed. Based on a coarsening kinetics model, used to relate the change in microstructure to the polarization resistance increase, the authors justified the degradation with surface diffusion limitation due to LSCF coarsening.

1.1.17.2. Cathode poisoning (Cr)

In 2009 Bentzen et al. [23] conducted an electrochemical study of composite LSCF-GDC cathode degradation by Cr poisoning. Two samples were tested in a 3-electrode set-up for 3000 h under current, 0.2 and 0.4 A/cm^2, at 850 and 750°C, in dry and 3% humidified air. One sample was placed in contact with a Cr_2O_3 pellet and the other one tested in a Cr-Free atmosphere. The EIS performed during testing under 0.2 A/cm^2 in dry and wet conditions revealed that the increase of the water partial pressure resulted in a degradation of the polarization resistance. At the same humidification level, instead, increasing the current density resulted in slower degradation most likely due to an increase of 20-30°C in temperature. The series resistance increased by 10-15% after 1000 h of operation. SEM/EDX observation showed no particular changes in microstructure between the Cr poisoned sample and the unexposed one except for a Cr containing phase that filled the pores causing the TPB blocking.

A comparison between LSCF and LSCF-GDC cathode under Cr poisoning conditions carried out by Zhao et al. [25] highlighted a higher tolerance of the composite cathode with respect to the single phase one. Because Cr deposits on the LSCF surface but not on GDC, the deposition of GDC nanoparticles allow avoiding direct contact between interconnect and the LSCF and thus to reduce the Cr deposition. LSCF and LSCF/GDC has been tested in presence of Fe-Cr metallic interconnect for 40 h at 800°C under cathodic polarization of 200 mA/cm^2. EIS measurement highlighted that while for LSCF Cr poisoning mainly affects the polarization resistance, for LSCF-GDC this contribution remains almost constant. Conversely, the ohmic resistance tends to increase slightly in the first 12 h and after it stabilized. SEM/EDX analysis on the composite electrode evidence that Cr was selectively deposited on LSCF rather than the GDC because of the interaction between Cr and segregated SrO.

Adjustment of the microstructure of the composite cathode is a potential strategy to improve the Cr tolerance. Recently Xiong et al. [24] correlated the Cr poisoning of LSCF-GDC to the sintering temperature of the composite cathode by an EIS analysis combined with SEM/EDX observations. It is known that increasing the sintering temperature increases the particles connection between the two materials and at the same time reduces the porosity and the specific surface area for reaction. In concordance with this assessment, the authors

achieved a decrease of the degradation of both the ohmic and the polarization resistances of symmetrical cell GDC/LSCF-GDC (1:1 by weight) by increasing the sintering temperature (ageing for 200 h in the presence of a Fe-Cr interconnect). In particular, by separating the spectra in their components at low mid and high frequency, Cr degradation at low sintering temperature affects all its three components while at higher temperature it affects, to a lesser extent, mainly the low frequency arc. This contribution linked to the oxygen surface exchange reaction is inhibited by Cr deposition on the active surface of the cathode. The microstructure analysis revealed less Cr deposition for the samples sintered at higher temperature. In fact, increasing the sintering temperature reduces the reaction sites between Cr and SrO and at the same time, because of the lower porosity, the transport of Cr compounds in the cathode bulk is limited, preventing the passivation of the charge transfer process at the interface between cathode/electrolyte.

1.1.18. Bibliography

[1] J. Nielsen, T. Jacobsen, M. Wandel, Impedance of porous IT-SOFC LSCF:CGO composite cathodes, Electrochim. Acta. 56 (2011) 7963–7974. doi:10.1016/j.electacta.2011.05.042.

[2] K. Lu, F. Shen, Long term behaviors of La0.8Sr0.2MnO3 and La0.6Sr0.4Co0.2Fe0.8O3 as cathodes for solid oxide fuel cells, Int. J. Hydrogen Energy. 39 (2014) 7963–7971. doi:10.1016/j.ijhydene.2014.03.046.

[3] A. Mai, M. Becker, W. Assenmacher, F. Tietz, D. Hathiramani, E. Ivers-Tiffée, D. Stöver, W. Mader, Time-dependent performance of mixed-conducting SOFC cathodes, Solid State Ionics. 177 (2006) 1965–1968. doi:10.1016/j.ssi.2006.06.021.

[4] H. Yokokawa, H. Tu, B. Iwanschitz, A. Mai, Fundamental mechanisms limiting solid oxide fuel cell durability, J. Power Sources. 182 (2008) 400–412. doi:10.1016/j.jpowsour.2008.02.016.

[5] G. Constantin, C. Rossignol, P. Briois, a. Billard, J.-P. Barnes, L. Dessemond, E. Djurado, Influence of Gadolinia-Doped Ceria Buffer Layer on the Durability of LSCF/CGO/YSZ System for IT-SOFC, ECS Trans. 45 (2012) 295–305. doi:10.1149/1.3701319.

[6] M. Shah, P.W. Voorhees, S.A. Barnett, Time-dependent performance changes in LSCF-infiltrated SOFC cathodes: The role of nano-particle coarsening, Solid State Ionics. 187 (2011) 64–67. doi:10.1016/j.ssi.2011.02.003.

[7] Y.T. Kim, Z. Jiao, N. Shikazono, Evaluation of La0.6Sr0.4Co0.2Fe0.8O3-Gd0.1Ce0.9O1.95 composite cathode with three dimensional microstructure reconstruction, J. Power Sources. 342 (2017) 787–795. doi:10.1016/j.jpowsour.2016.12.113.

[8] A. Weber, J. Szász, S. Dierickx, C. Endler-schuck, E. Ivers-tiffée, Accelerated Lifetime Tests for SOFCs, ECS Trans. 68 (2015) 1953–1960. doi:10.1149/06801.1953ecst.

[9] R.R. Mosbæk, Solid Oxide Fuel Cell Stack Diagnostics, Department of Energy Conversion and Storage Ph . D . Thesis, 2014.

[10] Z. Wuillemin, Y. Antonetti, C. Beetschen, O. Millioud, S. Ceschini, H. Madi, J. Van herle, Local Activation and Degradation of Electrochemical Processes in a SOFC, ECS Trans. 57 (2013) 561–570. doi:10.1149/05701.0561ecst.

[11] M. Hubert, J. Laurencin, P. Cloetens, J.C. da Silva, F. Lefebvre-Joud, P. Bleuet, A. Nakajo, E. Siebert, Role of microstructure on electrode operating mechanisms for mixed ionic electronic conductors: From synchrotron-based 3D reconstruction to electrochemical modeling, Solid State Ionics. 294 (2016) 90–107. doi:10.1016/j.ssi.2016.07.001.

[12] C. Endler-Schuck, A. Leonide, A. Weber, S. Uhlenbruck, F. Tietz, E. Ivers-Tiffée, Performance analysis of mixed ionic-electronic conducting cathodes in anode supported cells, J. Power Sources. 196 (2011) 7257–7262. doi:10.1016/j.jpowsour.2010.11.079.

[13] C. Pellegrinelli, Y.L. Huang, J.A. Taillon, L.G. Salamanca-Riba, E.D. Wachsman, Investigating the Relationship Between Operating Conditions and SOFC Cathode Degradation, ECS Trans. 68 (2015) 773–784. doi:10.1149/06801.0773ecst.

[14] R.R. Liu, S.H. Kim, S. Taniguchi, T. Oshima, Y. Shiratori, K. Ito, K. Sasaki, Influence of water vapor on long-term performance and accelerated degradation of solid oxide fuel cell cathodes, J. Power Sources. 196 (2011) 7090–7096. doi:10.1016/j.jpowsour.2010.08.014.
[15] J. Nielsen, A. Hagen, Y.L. Liu, Effect of cathode gas humidification on performance and durability of Solid Oxide Fuel Cells, Solid State Ionics. 181 (2010) 517–524. doi:10.1016/j.ssi.2010.02.018.
[16] Y. Yu, H. Luo, D. Cetin, X. Lin, K. Ludwig, U. Pal, S. Gopalan, S. Basu, Effect of atmospheric CO2 on surface segregation and phase formation in La0.6Sr0.4Co0.2Fe0.8O3-δ thin films, Appl. Surf. Sci. 323 (2014) 71–77. doi:10.1016/j.apsusc.2014.09.019.
[17] J.S. Hardy, J.W. Templeton, D.J. Edwards, Z. Lu, J.W. Stevenson, Lattice expansion of LSCF-6428 cathodes measured by in situ XRD during SOFC operation, J. Power Sources. 198 (2012) 76–82. doi:10.1016/j.jpowsour.2011.09.099.
[18] H. Wang, K.J. Yakal-Kremski, T. Yeh, G.M. Rupp, A. Limbeck, U. Fleig, S.A. Barnett, Mechanisms of Performance Degradation of (La,Sr)(Co,Fe)O 3-δ Solid Oxide Fuel Cell Cathodes, J. Electrochem. Soc. 163 (2016) 581–585. doi:10.1149/2.0031607jes.
[19] F. Shen, K. Lu, Moisture effect on La0.8Sr0.2MnO3 and La0.6Sr0.4Co0.2Fe0.8O3 cathode behaviors in solid oxide fuel cells, Fuel Cells. 15 (2015) 105–114. doi:10.1002/fuce.201400032.
[20] N. Ni, S.J. Cooper, R. Williams, N. Kemen, D.W. McComb, S.J. Skinner, Degradation of (La 0.6 Sr 0.4) 0.95 (Co 0.2 Fe 0.8)O 3−δ Solid Oxide Fuel Cell Cathodes at the Nanometer Scale and below, ACS Appl. Mater. Interfaces. 8 (2016) 17360–17370. doi:10.1021/acsami.6b05290.
[21] [21] D.-H. Cho, H. Kishimoto, K. Yamaji, M.E. Brito, K.D.- Bagarinao, M. Nishi, T. Shimonosono, F. Wang, H. Yokokawa, T. Horita, Evaluation of the Cathode Performance and the Distribution of Deposited Cr Species in the LSCF6428 Cathode by Cr Poisoning, ECS Trans. 57 (2013) 1865–1872. doi:10.1149/05701.1865ecst.
[22] D. Oh, E. Armstrong, D. Jung, C. Kan, E. Wachsman, Mechanistic Understanding of Cr Poisoning on La0.6Sr0.4Co0.2Fe0.8O3-δ (LSCF), ECS Trans. 25 (2009) 2871–2879.
[23] J.J. Bentzen, J.V.T. H??gh, R. Barfod, A. Hagen, Chromium poisoning of LSM/YSZ and LSCF/CGO composite cathodes, Fuel Cells. 9 (2009) 823–832. doi:10.1002/fuce.200800143.
[24] C. Xiong, J.A. Taillon, C. Pellegrinelli, Y.-L. Huang, L.G. Salamanca-Riba, B. Chi, L. Jian, J. Pu, E.D. Wachsman, Long-Term Cr Poisoning Effect on LSCF-GDC Composite Cathodes Sintered at Different Temperatures, J. Electrochem. Soc. 163 (2016) F1091–F1099. doi:10.1149/2.0841609jes.
[25] L. Zhao, S. Amarasinghe, S.P. Jiang, Enhanced Chromium Tolerance of Gd0.1Ce0.9O1.95 Impregnated La0.6Sr0.4Co0.2Fe0.8O3-δ Electrode of Solid Oxide Fuel Cells, ECS Trans. 57 (2013) 2163–2173.
[26] M. Perz, E. Bucher, C. Gspan, J. Waldhäusl, F. Hofer, W. Sitte, Long-term degradation of La0.6Sr0.4Co0.2Fe0.8O3-δ IT-SOFC cathodes due to silicon poisoning, Solid State Ionics. 288 (2015) 22–27. doi:10.1016/j.ssi.2016.01.005.
[27] F. Wang, K. Yamaji, D.-H. Cho, T. Shimonosono, H. Kishimoto, M.E. Brito, T. Horita, H. Yokokawa, Sulfur Poisoning on La0.6Sr0.4Co0.2Fe0.8O3 Cathode for SOFCs, J. Electrochem. Soc. 158 (2011) B1391. doi:10.1149/2.059111jes.
[28] R.-R. Liu, S. Taniguchi, Y. Shiratori, K. Ito, K. Sasaki, Influence of SO2 on the Long-term Durability of SOFC Cathodes, ECS Trans. 35 (2011) 2255–2260. doi:10.1149/1.3570221.
[29] W. Zhang, Investigation of Degradation Mechanisms of LSCF based SOFC cathodes - by CALPHAD modeling and experiments, Dep. Energy Convers. Storage. PhD (2012) 231. http://orbit.dtu.dk/ws/files/52717277/Investigation_of_Degradation_Mechanisms.pdf.

[30] S.P. Jiang, X. Chen, Chromium deposition and poisoning of cathodes of solid oxide fuel cells - A review, Int. J. Hydrogen Energy. 39 (2014) 505–531. doi:10.1016/j.ijhydene.2013.10.042.

1.8. EIS on SOFC: Fuel Cross Over

UNISA, CEA

1.1.19. Introduction

During operation of a Solid Oxide Fuel Cell, one of the operational losses is fuel crossover, which leads to a mixed potential on the cathode side. This loss is associated with the losses that might occur thought the electrolyte. It may be caused by pin holes in the ceramic electrolyte [1].

A leakage of air into the anode side is favored because of the high air flow with respect to the fuel flow, if no pressure difference is ensured between anode and cathode compartment. If the slight overpressure in the fuel side is lost, a leak of air into the anode side may cause an increase in temperature, due to parasitic hydrogen combustion that might not be detected, as the probability is high that it happens in some distance from the next thermocouple. And even more problematic is the risk of Ni-reoxidation in cases of high fuel utilizations. The overall effect of gas leak consists of a loss of potential due to the parasitic reaction that produces water and in a volumetric loss which increases the fuel utilization.

In case of a leakage from cathode to anode side, one can estimate the loss of fuel across the membrane by checking the OCV deviation from the theoretical EMF calculated by the Nernst equation. Some hints of a leakage happening in the stack should be noted in the I-V curve measurements [2]. Fuel loss due to internal shorting of Ceria and Samaria-Doped Ceria (SDC) electrolytes becomes a significant concern when it is used in applications requiring high fuel utilization and electrical efficiency [3]. Therefore, YSZ-electrolytes are utilized in most applications.

1.1.20. Leakages in a SOFC

A SOFC can have both internal leakages between anode and cathode (when the fuel reaches the cathode side, known as anodic leakage, or when the air reaches the anode one, known as cathodic leakage) and external leakages between the cell itself and the surrounding. At a system level, in addition to the loss of performance, a leakage might affect the heat production between elements of the balance of plant, in fact, for example, in case of fuel leakage a smaller amount of fuel is provided to the post burner connected to the stack and thus decreasing its temperature.

Leakages are driven by the pressure and by the different concentrations between the cathode and the anode, which push the fuel or the air to cross the electrode and reach the other side to react with respectively the fresh air or the fuel [4] [5].

Depending on the main cause, a leakage can be classified as viscous or diffusive: a viscous leakage is driven by different pressures between cathode and anode and then keeps constant the composition of two gases, while a diffusive leakage is driven by difference on concentrations, then it is possible to have a mixed leakage in which both fuel and air cross the electrode [6].

Reactions occurring due to an internal leakage are accelerated by high operating temperatures and by the presence of catalytic active materials, which lead to an immediate reaction, causing the instantaneous formation of hotspots in the cell.

According to these reactions anodic leakage involves the production of carbon dioxide and steam as described in equations 1-3, while cathodic leakage involves the oxidation of flammable substances at the anode.

$$CH_4 + 2O_2 \rightarrow CO_2 + 2H_2O \quad (1)$$

$$CO + \tfrac{1}{2}O_2 \rightarrow CO_2 \quad (2)$$

$$H_2 + \tfrac{1}{2}O_2 \rightarrow 2H_2O \quad (3)$$

Thus, it is fundamental to detect the presence and the amount of leakages.

1.1.21. Leakage monitoring

The literature lacks studies on monitoring and quantifying the leakage occurring in the cell, especially through EIS methodology. The scientific community focuses on different materials adopted for sealing, in order to prevent the fault instead of implementing methodologies aiming at mitigating the fault [6].

Of course, the leakage is usually due to a physical breakdown of the system, thus fault mitigation could be not very effective. Studies on different sealing methodologies can be found in [7] where authors studied the behaviour of different sealant for leakage test, stating that Mica paper have highly attractive features for sealing purposes, in [8] where sealing tests were carried out at 800 °C with simulated fuel cell anode gas, in particular focusing on Thermiculite 866 and Statotherm HT, in [9] where authors worked on metallic materials and their deformation, in order to understand their effects on the arise of leakages, and in [10] where an electron-blocking layer was incorporated at the anode/electrolyte interface, and results proved that the cell worked at high fuel utilization and low temperatures with a negligible internal short circuit and leakage.

Ways of detecting a leakage, especially a fuel crossover are actually under investigation by the scientific community. Stack leakages have been assessed qualitatively by observing changes in stack temperature [11], voltage and gas composition [12]. For this purpose, online and in situ methodologies to detect and quantify stack leakages would be beneficial both for distinguishing them from other detrimental phenomena causing stack degradation (e.g. Sulphur poisoning) and for individuating the right fault mitigation, if possible, to implement.

As Rautanen [8] reported, leakages can cause cell degradation by means of several mechanisms, e.g. increased thermal gradients [13], local shortage of fuel, oxidation of the anode and increased chromium evaporation [14] due to higher water vapor content at the cathode. Typically, glass-ceramics also require a specific heat treatment in which binder is evaporated and a stable phase is formed. Chemical reactions have also been reported between glass-ceramics and other stack components. These reactions can include cross-diffusion [15] and excessive surface and internal oxidation at steel-sealant interface [16] as well as increased chromium evaporation from interconnect steels [17].

As Bram et al. stated [9], internal leakage can lead nickel to re-oxidation especially with mixture characterized by high dilution, leading to exothermal reaction and then sever damages due to the formation of the so called hot spots; moreover leakages might cause fuel starvation due to the increasing in the fuel utilization.

As regards the measurement, Rasmussen et al [4] proposed an experimental method for the investigation of external and internal gas leaks occurring during a test of cells in a sealed setup. In the study of internal leaks, they added He or Ar to the fuel and then analyzed the air outlet. In particular, they measured the pO_{2in} and the pO_{2out} voltage and the cell voltage under different flows and compared these values to the theoretical EMF of the fuel gas mixture deduced from the known hydrogen content and thus evaluating leak currents. They found that the internal gas leak did not depend on the pressure difference between the anode and the cathode side, and it might be described as diffusion driven.
Anodic leakages are usually detected by observing the changes in gas composition through a sensor ad hoc (difficult to implement on-board) which detects the fault according to equations (1-3). It is worth remarking that cathodic leakages can be found through the N_2 composition monitoring. In fact, if fresh air crosses the electrode and reaches the anode side, the O_2 immediately reacts with the fuel entering the anode. Thus, an increase in temperature associated to the reaction, generates a hotspot in that point that might not be detected by sensors, if installed far away from the fault. While O_2 reacts with fuel at the anode side, N_2 is just an inert gas, and it concurs only at increasing the total mass leaving the anode. Thus, monitoring the outlet composition, an anomalous variation in the total gas mass could be the hint of a cathodic leakage happening in the cell.

Based on these conclusions, a model based approach might be useful to implement a detection analysis by individuating how composition and temperature could be correlated to symptoms in order to detect a fault leakage. In this field, Yang et al. [18] realized an electrochemical model accounting for the probability of crossover fault (around 0.9), which reduces the voltage trough a simplified Arrhenius approach on the evaluation of the voltage. Sorce et al. [19] implanted faults in an experimental SOFC system taking under consideration, among the faults, fuel and air leakage, and monitored their effect on the overall performances in terms of power, temperature and air flow rate. Even if they discussed about external leakages, the same approach might be adopted for the internal one, and then for the fuel crossover. Moreover, it is worth remarking the work done by Halinen [6], where a study of an in-situ leakage analysis in a planar SOFC was performed. In particular they experimentally quantified leakages at nominal operating conditions by means of composition analysis and monitoring fuel and air compositions. In parallel they developed a diffusive leakage model to quantify the leakage amount, showing how a model based approach might be useful for fault identification aiming at discriminating against a loss of tension between this phenomenon and another degradation mechanism.

1.1.22. Bibliography

[1] Singhal, S. C., & Kendall, K. (Eds.). (2003). *High-temperature solid oxide fuel cells: fundamentals, design and applications*. Elsevier.

[2] Boaro, M., & Aricò, A. S. (2017). *Advances in Medium and High Temperature Solid Oxide Fuel Cell Technology*. Springer.

[3] Zhang, X., Robertson, M., Deĉes-Petit, C., Qu, W., Kesler, O., Maric, R., & Ghosh, D. (2007). Internal shorting and fuel loss of a low temperature solid oxide fuel cell with SDC electrolyte. *Journal of Power Sources*, *164*(2), 668-677.

[4] Rasmussen, J. F. B., Hendriksen, P. V., & Hagen, A. (2008). Study of Internal and External Leaks in Tests of Anode-Supported SOFCs. *Fuel Cells*, *8*(6), 385-393.

[5] Wuillemin, Z., Autissier, N., Nakajo, A., Luong, M., & Favrat, D. (2008). Modeling and study of the influence of sealing on a solid oxide fuel cell. *Journal of fuel cell science and technology*, *5*(1), 011016.

[6] Halinen, M., & Pennanen, J. (2015). Analysis of leakages in a solid oxide fuel cell stack in a system environment. *Fuel cells*, *15*(2), 434-444.

[7] Nguyen, X. V., Chang, C. T., Jung, G. B., Chan, S. H., Lee, W. T., Chang, S. W., & Kao, I. C. (2016). Study of sealants for SOFC. *International Journal of Hydrogen Energy*, *41*(46), 21812-21819.

[8] Rautanen, M., Himanen, O., Saarinen, V., & Kiviaho, J. (2009). Compression Properties and Leakage Tests of Mica-Based Seals for SOFC Stacks. *Fuel Cells*, *9*(5), 753-759.

[9] Bram, M., Reckers, S., Drinovac, P., Mönch, J., Steinbrech, R. W., Buchkremer, H. P., & Stöver, D. (2004). Deformation behavior and leakage tests of alternate sealing materials for SOFC stacks. *Journal of Power Sources*, *138*(1), 111-119.

[10] Sun, W., & Liu, W. (2012). A novel ceria-based solid oxide fuel cell free from internal short circuit. *Journal of Power Sources*, *217*, 114-119.

[11] Blum, L., Packbier, U., Vinke, I. C., & de Haart, L. G. J. (2013). Long-Term Testing of SOFC Stacks at Forschungszentrum Jülich. *Fuel Cells*, *13*(4), 646-653.

[12] George, R. A. (2000). Status of tubular SOFC field unit demonstrations. *Journal of Power Sources*, *86*(1), 134-139.

[13] Fergus, J. W. (2005). Sealants for solid oxide fuel cells. *Journal of Power Sources*, *147*(1), 46-57.

[14] Stanislowski, M., Wessel, E., Hilpert, K., Markus, T., & Singheiser, L. (2007). Chromium vaporization from high-temperature alloys I. Chromia-forming steels and the influence of outer oxide layers. *Journal of the Electrochemical Society*, *154*(4), A295-A306.

[15] Yang, Z., Meinhardt, K. D., & Stevenson, J. W. (2003). Chemical compatibility of barium-calcium-aluminosilicate-based sealing glasses with the ferritic stainless steel interconnect in SOFCs. *Journal of the Electrochemical Society*, *150*(8), A1095-A1101.

[16] Batfalsky, P., Haanappel, V. A. C., Malzbender, J., Menzler, N. H., Shemet, V., Vinke, I. C., & Steinbrech, R. W. (2006). Chemical interaction between glass–ceramic sealants and interconnect steels in SOFC stacks. *Journal of Power Sources*, *155*(2), 128-137.

[17] Ogasawara, K., Kameda, H., Matsuzaki, Y., Sakurai, T., Uehara, T., Toji, A., ... & Yokokawa, H. (2007). Chemical stability of ferritic alloy interconnect for SOFCs. *Journal of the Electrochemical Society*, *154*(7), B657-B663.

[18] Yang, J., Li, X., Jiang, J. H., Jian, L., Zhao, L., Jiang, J. G., ... & Xu, L. H. (2011). Parameter optimization for tubular solid oxide fuel cell stack based on the dynamic model and an improved genetic algorithm. *International Journal of Hydrogen Energy*, *36*(10), 6160-6174.

[19] Sorce, A., Greco, A., Magistri, L., & Costamagna, P. (2014). FDI oriented modeling of an experimental SOFC system, model validation and simulation of faulty states. *Applied Energy*, *136*, 894-908

1.9. SOFC: Estimation of State of Health

DTU, Alexandra Ploner

1.1.23. Introduction

In order to detect and diagnose cell and stack failures modes, it is necessary to monitor the system and to estimate the state-of-health (SoH). The main purpose of the SoH parameter is to evaluate the deviation from the 'normal' and the 'faulty' state. As the SoH does not correspond to a specific physical quantity and rather reflects the general condition of the stack and system, different indicators may be used to derive the SoH. Diagnosis methods either rely on additional sensors added to the stack/system to derive the SoH parameter or the diagnosis procedure makes use of the stack as its own sensor [1]. This literature study aims to review the various concepts for SoH evaluation for the SOFC technology.

The activities carried out on different health management tools for SOFCs can be categorized into (i) model-based [2,3,4,5,6,7,8,9,10,11] [12,13,14] and (ii) signal-based detection method [15,16] to estimate the SoH. Similarly, this has been done for PEMFC (Polymer Electrolyte Membrane fuel cell) [17].

1.1.24. Model-based detection of SOH

Model-based detection methods are commonly also referred to as residual-based methods, as the variable monitored on the real system (Y) is compared with the variable generated by the model($\hat{Y}$) (= residuals).

$$r = \frac{Y-\hat{Y}}{\hat{Y}} \cdot 100 \qquad (1)$$

Theoretically, if an accurate model is used, the residuals between simulation and real system are equal to zero. However, uncertainties related to the model along with disturbances and noise connected to the experimental measurement lead to nonzero residuals. Thus, the computed residuals may lie in a tolerance range even at nominal operating condition. Consequential, residuals overcoming the specified thresholds might indicate a possible fault [18]. In this context, the residual range specifies the SoH.

Different model approaches can be considered i.e. physical modeling, grey-box modeling or black-box modeling. A detailed review (2013) on various models in correlation with fault diagnostic for SOFCs can be found in Ref. [19]. Additionally, a recent (2016) book [18] was released summarizing model-based diagnostic approaches for SOFC in chapter 4.

Among the model-based approaches the EIS technique takes up a special position. It is a widespread and powerful technique able to identify various phenomena inside the electrochemical system and to investigate its changes. The general idea is to analyze the system responses towards a sinusoidal imposed perturbation. The obtained data is then subjected to modelling. Based on physical and (electro-)chemical process of the investigated system an equivalent-circuit model is constructed in order to diagnose the different processes involved.

Gazzarri et al. [20] developed a finite element model to simulate the impedance response of an intact SOFC (nominal conditions) and delaminated cell (faulty condition). The impact of delamination on the EIS was computed by an array of elements with the dielectric properties of air. In an additional studies by Gazzarri the model was extended to simulate other degradation phenomena (chromium poisoning, sulfur poisoning, anode nickel sintering) [21] and rib detachment [22].

SOFC impedance responses were furthermore modeled by Prasad et al. [23]. The model simulated the impedance response of a button cell affected by sulfur poisoning, but with no particular focus on fault diagnosis.

1.1.25. Signal-based detection of SoH

Signal-based detection methods firstly depend on a chosen signal derived from the system and secondly an efficient signal analysis method for interpreting. This methodology furthermore relies on

a data set for nominal operating and defective operating conditions. This data may be derived from laboratory test benches or on-field used systems. For SOFC health diagnostic, two measurements are primarily considered (i) fault detection by Electrochemical Impedance Spectra (EIS) technique [24,25] and (ii) fault detection by current or voltage transformation [16,15].

1.1.26. SoH determined by EIS

The use of on-line EIS measuring of the fuel cell stack requires an (i) appropriate setup, (ii) a substantial database on EIS measurements and an (iii) algorithm performed on selected features of the EIS data. To the best of our knowledge, literature concerning data processing algorithms is rather limited.

Das [24] performed SoH monitoring via EIS on a sub-commercial 5-cell stack. Performance with regard to different operation conditions i.e. H_2/CO fuel, steam-to-carbon (S/C) ratio and fuel utilization (FU) were evaluated and the SoH was investigated for eight possible combinations in a period of 500 h at 0.4 A cm^{-2}.

Moreover, Mosbæk [25]evaluated performance, degradation and the SoH of a 13-cell stack (2500 h) and a 14-cell stack (667 h) under nominal operation conditions. Stack 1 was operated at 750°C, 52% FU, H2-fuel and 0.2 A cm^{-2} and stack 2 at 720°C, 56% FU, 50/50 H_2/H_2O fuel and 0.2 A cm^{-2}, respectively.

1.1.27. SoH determined by measured voltage

From the industrial point of few this approach has the advantage to use the stack as a sensor itself and no particular setup for monitoring is needed.

Pahon et al. [16], for example, presented a signal-based on continuous wavelet transformation of the monitored stack voltage. The retrieved SoH parameters are relative wavelet energy (RWE) and total wavelet entropy (TWP) and relative wavelet entropy (RWP). For the experiment, a 6 cell stack was tested under nominal and non-nominal conditions according to the design of experiment approach. 16 tests were performed by variation of 4 parameter i.e. fuel utilization, air utilization, current density and temperature to collect characteristic voltage data under steady-state conditions. Additionally, an ageing test (1677 h) on a 3 cell-stack was conducted to evaluate the different SoH indicators. Based on the two experiments the author concluded that the RWP is the most effective indicator for the SoH of a SOFC, by allowing a detection of the fuel cell damages and also by well-fitting an ageing phenomenon.

Furthermore, in the work of Esposito et al. [15] the continuous wavelet transform methodology is used. Their work is focusing on possible detection of anode re-oxidation induce by locally high FU. A qualitative analysis was carried out by comparing the CWT treated signals at different FUs while a quantitative comparison was performed by CWT matrix coefficients.

Results of long-term voltage degradation testing of different stack configurations – however with no specific focus on SoH assessment – can be found in Ref. [26,27,28]. This might help to establish a database with respect to stack operation at nominal conditions.

1.1.28. Bibliography

[1] A. R. Isermann in Fault-Diagnosis Systems: An Introduction from Fault Detection to Fault Tolerance, Springer-Verlag Berlin Heidelberg, 2006.

[2] P. Costamagna, A. D. Giorgi, L. Magistri, G. Moser, L. Pellaco, A. Trucco, IEEE Transactions on Energy Conversion 2016, 31, 676-687.

[3] Z. Deng, H. Cao, X. Li, J. Jiang, J. Yang, Y. Qin, J. Power Sources 2010, 195, 8097-8103.

[4] L. Pellaco, P. Costamagna, A. D. Giorgi, A. Greco, L. Magistri, G. Moser, A. Trucco, Electron. Lett. 2014, 50, 824-826.

[5] P. Polverino, A. Esposito, C. Pianese, B. Ludwig, B. Iwanschitz, A. Mai, J. Power Sources 2016, 306, 646-657.

[6] P. Polverino, C. Pianese, M. Sorrentino, D. Marra, Journal of Power Sources 2015, 280, 320-338.
[7] A. Sorce, A. Greco, L. Magistri, P. Costamagna, Appl. Energy 2014, 136, 894-908.
[8] X. Wu, D. Gao, Int. J. Hydrogen Energy 2017, 42, 2288-2308.
[9] D. Marra, M. Sorrentino, C. Pianese, B. Iwanschitz, J. Power Sources 2013, 241, 320-329.
[10] A. Pohjoranta, M. Sorrentino, C. Pianese, F. Amatruda, T. Hottinen, Energy Procedia 2015, 81, 173-181.
[11] X. Wu, Q. Ye, J. Power Sources 2016, 321, 47-56.
[12] J. T. Allen, N. H. El-Farra, Renew. Energy 2017, 100, 35-43.
[13] U. K. Chakraborty, Energy 2009, 34, 740-751.
[14] M. Linder, T. Hocker, C. Meier, L. Holzer, K. A. Friedrich, B. Iwanschitz, A. Mai, J. A. Schuler, Journal of Power Sources 2015, 288, 409-418.
[15] A. Esposito, L. Russo, C. Kändler, C. Pianese, B. Ludwig, N. Y. Steiner, J. Power Sources 2016, 317, 159-168.
[16] E. Pahon, N. Yousfi Steiner, S. Jemei, D. Hissel, M. C. Péra, K. Wang, P. Mocoteguy, Int. J. Hydrogen Energy 2016, 41, 13678-13687.
[17] D. Hissel, M. C. Pera, Annual Reviews in Control 2016, 42, 201-211.
[18] D. Marra, C. Pianese, P. Polverino, M. Sorrentino in Models for Solid Oxide Fuel Cell Systems, Springer-Verlag London, 2016.
[19] K. Wang, D. Hissel, M. C. Péra, N. Steiner, D. Marra, M. Sorrentino, C. Pianese, M. Monteverde, P. Cardone, J. Saarinen, Int. J. Hydrogen Energy 2011, 36, 7212-7228.
[20] J. I. Gazzarri, O. Kesler, J. Power Sources 2007, 167, 430-441.
[21] J. I. Gazzarri, O. Kesler, J. Power Sources 2007, 167, 100-110.
[22] J. I. Gazzarri, O. Kesler, J. Power Sources 2008, 176, 138-154.
[23] B. V. R. S. N. Prasad, V. M. Janardhanan, Journal of The Electrochemical Society 2014, 161, F208--F213.
[24] D. Das, Ph.D. dissertation, The Pennsylvania State University, 2016.
[25] R. R. Mosbæk, J. Hjelm, P. V. Hendriksen, R. G. Barfod, Ph.D. dissertation, Department of Energy Conversion and Storage, Technical University of Denmark, 2014.
[26] L. Blum, U. Packbier, I. C. Vinke, L. G. J. de Haart, Fuel Cells 2013, 13, 646-653.
[27] M. Yoshikawa, T. Yamamoto, K. Yasumoto, Y. Mugikura, ECS Transactions 2017, 75, 23-31.
[28] J. Hong, H.-J. Kim, S.-Y. Park, J.-H. Lee, S.-B. Park, J.-H. Lee, B.-K. Kim, H.-J. Je, J. Y. Kim, K. J. Yoon, International Journal of Hydrogen Energy 2014, 39, 20819-20828.

1.10. PEM and other electrochemistry related active diagnostic methods

IJS, Dani Juricic

The conventional EIS approach relies on single sine excitation or frequency sweep using linear or logarithmic steps [1]. Three conditions must be fulfilled for correct evaluation of the EIS spectra: (i) causality, (ii) linearity and (iii) time invariance. Failure to meet these requirements might result in distorted (biased) or even misleading EIS spectra. The limitations of the single sine approach are mainly twofold.

Given the fact that electrochemical systems are in general governed by Buttler-Volmer's equation, they are nonlinear [1]. In order not to violate linearity, the amplitude of the excitation sine waveforms should be taken low enough, which in turn decreases signal-to-noise ratio and hence quality of the evaluated EIS curves.
Repetitive use of single sines can result in long experiments, especially due to the points in the low frequency part of the EIS curve. Moreover, in the mHz range the problem might be to guarantee the time invariant properties of the operating conditions as well as internal condition of the system.

To avoid the first problem, various linearity assessment methods can be applied like (i) the experimental methods (AC plots and Lissajous plots), (ii) methods employing the harmonic analysis of the response signal and (iii) methods based on the Kramers-Kronig relations [1] and hereupon based methods, cf. [2,3].

Instead of using single sine waves one by one, an excitation signal made as a sum of sines at different frequencies can be applied. In this way, the measurement time can be significantly shorter than for one-by-one frequency measurements. Such waveforms are referred to as multi-sine signals.

If a continuum of the constituent sine waves is applied, i.e. at all the frequencies from a part or a whole frequency range, such an excitation signal is referred to as a *broadband signal*. However, the biggest disadvantage of the broadband probing signals for EIS applications is the decrease in accuracy (signal to noise ratio) of the impedance spectrum and in impedance sensitivity in favor of the increased measuring speed [1]. Some broadband excitation signals are proposed and explained in detail in the following sections.
Multi-sine and broadband excitation signals have encountered a range of applications in PEM fuel cells as well as some other electrochemical processes like corrosion monitoring. Subsequent, the main unconventional EIS-oriented ideas and some of the accomplishments will be reviewed.

1.1.29. EIS based on multi-sine excitation signals

Unlike the classical EIS technique, which uses a single frequency probing u(t)=A sin(2πft), a multi-sine excitation signal uses the sum of harmonics:

$$u(t) = \sum_{k=1}^{N} A_k sin(2\pi f_k t + \varphi_k) \qquad (1)$$

where A_k are the amplitudes, f_k frequencies and φ_k the phases of the sine functions applied. Time needed to take the measurements is equal to the period of the lowest frequency used in the signal in Eq. 1.

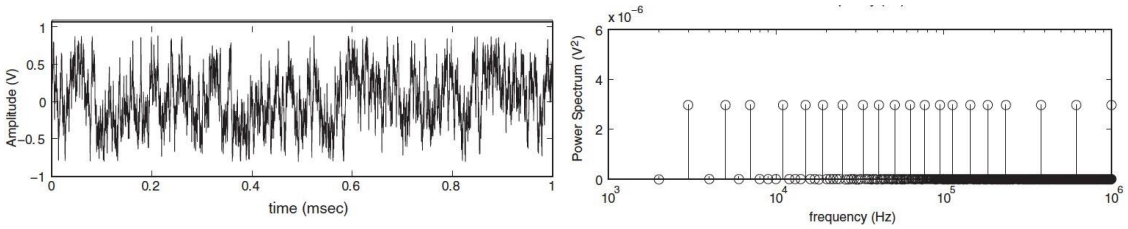

Figure 7: Multi-sine signal in time domain (A) and its amplitude power spectrum (B) [5]

Figure 7 represents an example of a multi-sine perturbation signal in time domain and its power spectrum. The main advantage of using multi-sine probing signal for EIS purposes, when comparing to the rest of the probing signals, is the flexibility to directly specify the excitation power spectrum (amplitudes and excited frequencies), which is mostly flat for the desired frequencies (Figure 7-B). However, the main disadvantage is that it cannot be used without previous optimization of the phases in time domain. The main problem of the non-optimized multi-sine signal is the possibility to exceed the maximum allowed amplitude of the signal in the linear region. There are several optimization approaches to avoid influence of non-linearities [4, 5, 6]. An example of using a multi-sine excitation signal to determine corrosion on aluminum alloys in NaCl solution is presented in [7]. In a recent work [8], an idea on how to select the frequency components as well as how to optimize their amplitudes in order to get optimal resolution and sensitivity of the transfer function.

1.1.30. Random phase excitation signal

The random phase signal is defined as in Eq. (1). However, what makes it interesting for EIS is the fact that the phase φ_k is uniformly distributed in the interval $[0,2\pi]$. In the time domain, the amplitudes of the random phase multi-sines look like normally distributed random noise (Figure 8 A) and that is the reason why they are commonly referred to as *periodic noise signal*. The amplitude spectrum of random noise signal is very similar to the white noise signal, which is flat. The only difference is the frequency spectrum of the random phase multi-sine signal is flat for the desired frequencies, not the whole spectrum [4, 6]. The approach has been applied to corrosion monitoring [6] where it is shown that the method is able to detect nonlinear modes of the process. It seems it is not researched so far how could EIS analysis of SOFCs benefit from the method due to high peak-to-peak value (crest factor).

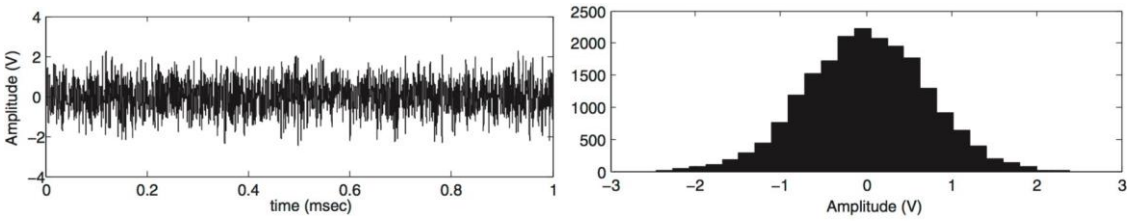

Figure 8: Random-phases multi-sine signal (A) and its amplitude histogram (B) [1]

1.1.31. Electrochemical frequency modulation

Electrochemical frequency modulation (EFM) is a technique which provides new tools mainly for electrochemical corrosion monitoring. It is a non-destructive technique similar to electrochemical impedance spectroscopy (EIS) which uses small signal AC perturbations. Both techniques (EIS and EFM) can be used to measure the corrosion rate. Unlike EIS, EFM uses two sine waves (with different frequencies) which are applied to the electrochemical system under test. Due to the nonlinear nature of the corrosion process, the potential perturbation of the sine waves will generate responses at more frequencies than the frequencies of the applied signals. Current responses can be measured at zero, harmonic and intermodulation frequencies [9, 10]. The principle of the EFM technique is illustrated in Figure 9. A schematic of a frequency spectrum of an EFM current response, illustrating the different harmonic and intermodulation frequencies, is presented in Figure 10.

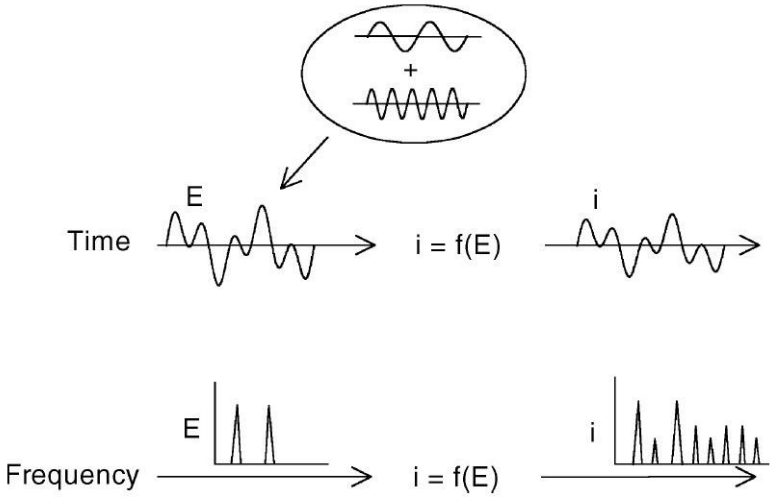

Figure 9: Principle of EFM [9]

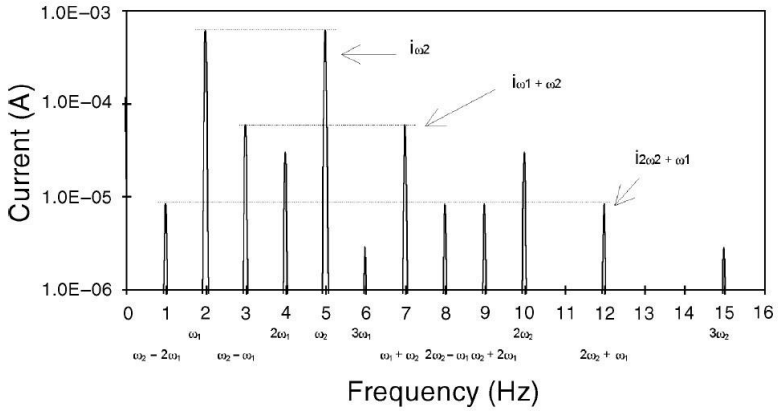

Figure 10: Harmonic and intermodulation frequencies resulting from the basic frequencies 2 Hz and 5 Hz [9]

According to Bosch et al. [9] EFM technique is capable of monitoring and detecting differences in the corrosiveness of the environment, like changes in the oxygen concentration and hydrodynamic conditions. Kus and Mansfeld [11] evaluated the EFM technique for several corrosion systems including active and passive systems and found that EFM measurements can be applied successfully only for a limited number of corrosion systems with fairly high corrosion rates. In spite of caution needed when using the technique, it seems it shares some similar features with the THD, which might be of interest to research.

1.1.32. EIS based on broadband excitation signals

1.1.32.1. Pulse excitation

Since it is easy to realize, system response to a pulse excitation can be used for quick characterization of Ohmic losses. In particular, it has been used to measure the PEM fuel cell membrane resistance *in time domain* [12, 13]. According to this method, the current passing through an external load is immediately set to 0, while the voltage output of the fuel cell is continuously observed. The voltage change due to the disappearance of the ohmic drop can be observed right away, while the voltage change due to the electrochemical overpotential gradually disappears (Figure 11).

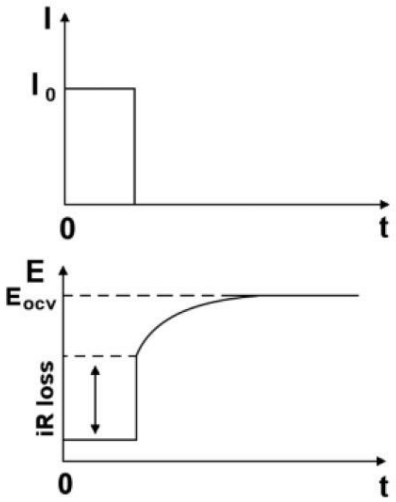

Figure 11: An ideal voltage transient in a fuel cell after current interruption [13]

1.1.32.2. Step excitation signal

Fourier transform of a pulse $h(t) = K\delta(t)$, where $\delta(t)$ is Dirac's delta function equals $H(j\omega) = K$. It contains all frequencies with the same amplitude K. However, such a function is impossible to be realized in practice because of the limitations in electronic and the fact that generated signal my damage the system under test. That is why Dirac pulse function is usually substituted by a pulse of short duration Δt. As it is difficult to apply very short pulse function, it is more convenient to apply step function and take its derivative which is Dirac's delta function. Such a method is used for determination of impedance [1], where authors also explained the need of high bit-resolution data acquisition systems in order not to lose valuable information from the system under test. Although the methods using pulse or step excitation are mathematically correct, their amplitudes at each frequency are quite weak, which are the main cause of their excessive sensitivity to noise [14].

1.1.32.3. Swept sine (chirp) excitation signal

Swept sine excitation signal is rapid sine sweep signal where the frequency is swept up and/or down in one measurement period. The sweeping is repeated in such a way where a periodic signal is created with the same period as the measurement period:

$$u(t) = sin\left[\left(\frac{\pi(f_2 - f_1)}{T}t + 2\pi f_1\right)t\right] \qquad (2)$$

where f_1 and f_2 represents respectively the minimum and maximum used frequency and T represents the measurement period.

According to Sanchez et al. [4] chirp excitations can be used in many ways depending on the frequency variation with time, however the most common uses a frequency swept up or down. An advantage of chirp signal is low crest factor, which helps keeping the signal amplitude in the linear regime. The main drawback is the lack of freedom to choose an arbitrary amplitude power spectrum. The chirp amplitude power spectrum is neither really flat at low frequencies, nor in the wanted frequency band, due to the ripple (Figure 12-B). The applicability to isolation flooding and drying in a PEM fuel cell is demonstrated by simulation [15].

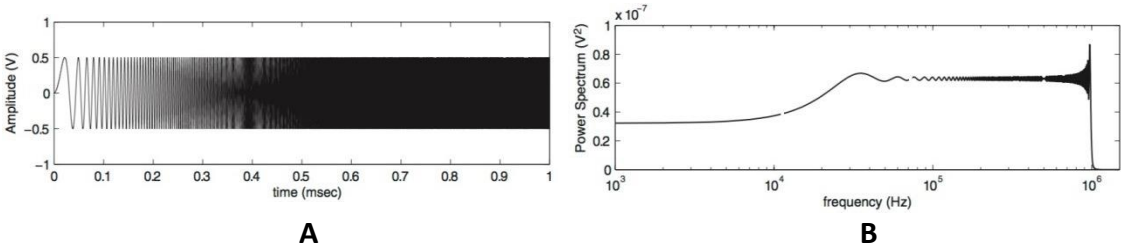

Figure 12: Up-chirp signal in time domain (A) and its power spectrum (B) [4]

1.1.32.4. Pseudorandom Binary signal (PRBS)

A way to retain the advantages of chirp excitation, while alleviating the unsatisfactory spectral properties, has been proposed in [16, 17]. The approach relies on pseudo-random binary sequence (PRBS), which is characterized by limited amplitude and uniform power spectrum in the lower part of the signal spectrum. According to Debenjak et al. [16] the maximum length PRBS is characterized by its order n, the maximum length period N, amplitude A and its sampling period Δt. The order n determines the maximum length period N (number of discrete points in time, when the PRBS signal can change its value):

$$N = 2^n - 1 \qquad (2)$$

However, the power spectrum of periodic PRBS with period N and sampling time Δt is defined:

$$\Phi\left(m\frac{2\pi}{N\Delta t}\right) = \frac{1}{N}\Phi^d(m)\left|\frac{sin\left(\frac{m\pi}{N}\right)}{\frac{m\pi}{N}}\right| \qquad (3)$$

where Φ^d represents the discrete power spectrum density Φ of maximum length PRBS signal with amplitude A and length N [16]. The power spectrum of the periodic PRBS is shown on the Figure 13. From this it can be seen that the amplitude of the power spectrum firstly reaches zero for frequency equal to the sampling frequency $f_s = 1/\Delta t$. Useful bandwidth of PRBS excitation signal is determined by the frequency f_B (Figure 13) which represents -3 dB drop from the nominal level.

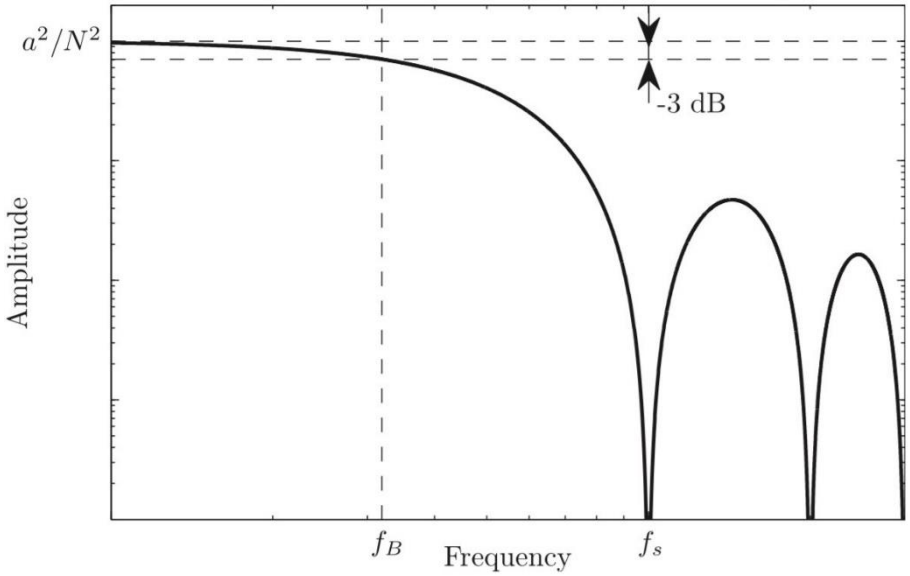

Figure 13: Power spectrum of the PRBS signal [16]

The main advantage of the PRBS over the single-sine is the shorter time period required for measurements. In [16] for measuring the impedance of the PEMFC from 0.1 Hz to 500 Hz, the measurements took 60 seconds to complete the EIS evaluation. The length of measurement time is tightly linked to the lower frequency limit of the frequency band, therefore only slightly higher limit (e.g. 0.5 Hz instead of 0.1 Hz) significantly shortens the required measurement time period.

To evaluate the EIS curve, the authors employ the idea of instantaneous impedance spectra (IIS) calculated by continuous wavelet transform (CWT) with Morlet mother wavelet. The idea of IIS has been originally suggested by Darowicki [18] who used Short-Time Fourier Transform in order to follow the time changes in spectra. The approach turned useful in electrode monitoring.

1.1.33. Bibliography

[1] A. Lasia, Electrochemical impedance spectroscopy and its applications, Springer, 2014.
[2] J. J. Giner-Sanz, E. M. Ortega, and V. Perez-Herranz, “Optimization of the perturbation amplitude for impedance measurements in a commercial PEM fuel cell using Total Harmonic Distortion,” Fuel Cells, vol. 16, no. 4, pp. 469–479, 2016.
[3] J. J. Giner-Sanz, E. M. Ortega, and V. Pérez-Herranz, “Application of a Monte Carlo based quantitative Kramers-Kronig test for linearity assessment of EIS measurements,” Electrochim. Acta, vol. 209, pp. 254–268, 2016.
[4] B. Sanchez, G. Vandersteen, R. Bragos, and J. Schoukens, “Basics of broadband impedance spectroscopy measurements using periodic excitations,” Measurement Science and Technology, vol. 23, no. 10, p. 105501, 2012.
[5] G. Popkirov and R. Schlinder, “The perturbation signal for fast fourier transform electrochemical impedance spectroscopy (fft-eis),” Bulg. Chem. Commun, vol. 27, pp. 459–67, 1994.
[6] J. Schoukens, R. Pintelon, E. Van Der Ouderaa, and J. Renneboog, “Survey of excitation signals for fft based signal analyzers,” IEEE Transactions on Instrumentation and Measurement, vol. 37, no. 3, pp. 342–352, 1988.
[7] E. Van Gheem, J. Vereecken, J. Schoukens, R. Pintelon, P. Guillaume, P. Verboven, and L. Pauwels, “Instantaneous impedance measurements on aluminium using a Schroeder multisine excitation signal,” Electrochimica Acta, vol. 49, no. 17, pp. 2919–2925, 2004.

[8] C. de Beer, P. S. Barendse and P. Pillay, Fuel cell condition monitoring using optimized broadband impedance spectroscopy. IEEE TRansactions on Industrial Electronics, vol. 62, no. 8, august 2015.
[9] R. Bosch, J. Hubrecht, W. Bogaerts, and B. Syrett, "Electrochemical frequency modulation: a new electrochemical technique for online corrosion monitoring," Corrosion, vol. 57, no. 1, pp. 60–70, 2001.
[10] S. Abdel-Rehim, K. Khaled, and N. Abd-Elshafi, "Electrochemical frequency modulation as a new technique for monitoring corrosion inhibition of iron in acid media by new thiourea derivative," Electrochimica Acta, vol. 51, no. 16, pp. 3269–3277, 2006.
[11] E. Ku¸s and F. Mansfeld, "An evaluation of the electrochemical frequency modulation (efm) technique," Corrosion Science, vol. 48, no. 4, pp. 965–979, 2006.
[12] M. Liu, J. Wang, S. Wang, X. Xie, T. Zhou, and V. Mathur, "On-line measurement for ohmic resistance in direct methanol fuel cell by current interruption method," Chinese Journal of Chemical Engineering, vol. 18, no. 5, pp. 843 – 847, 2010.
[13] X.-Z. R. Yuan, C. Song, H. Wang, and J. Zhang, "Impedance and its corresponding electrochemical processes," in Electrochemical Impedance Spectroscopy in PEM Fuel Cells: Fundamentals and Applications (X.-Z. R. Yuan, C. Song, H. Wang, and J. Zhang, eds.), pp. 95 – 139, Springer Science & Business Media, 2009.
[14] S.-M. Park and J.-S. Yoo, "Electrochemical impedance spectroscopy for better electrochemical measurements," 2003.
[15] L. Das, B. Srinivasan, and R. Rengaswamy, "On-line Performance Monitoring of PEM Fuel Cell using a Fast EIS Approach," 2015.
[16] A. Debenjak, P. Boskoski, B. Musizza, J. Petrovcic, and D. Juricic, "Fast measurement of proton exchange membrane fuel cell impedance based on pseudorandom binary sequence perturbation signals and continuous wavelet transform," Journal of Power Sources, vol. 254, pp. 112–118, 2014.
[17] P. Boskoski, A. Debenjak and B. Mileva Boshkoska, Fast Electrochemical Impedance Spectroscopy as a Statistical Condition Monitoring Tool. Springer, 2017
[18] K. Darowicki, Theoretical description of the measuring method of instantaneous impedance spectra, Journal of Electroanalytical Chemistry, Volume 486, Issue 2, 2000.

2. Summary

AVL, Stefan Pofahl

The effort spent so far to develop monitoring techniques for the operation of SOFC-based (micro-) CHP reflects the size of the market and the profit gained so far; - both are minor. This is reflected in this joint survey on the state of the art of diagnostic tools for this technology. A key point is the limited access to full stacks for researchers. Due to lack of resources for the scientific research on full stack level most of the researchers focus on investigations on single cells and small stack level in a controlled environment of test beds. Descriptions of monitoring tools suitable for implementation in commercial SOFC-systems is hard to find. This is not an outcome of this study, it is a confirmation of the motivation for the INSIGHT project and its predecessors GENIUS, DESIGN and DIAMOND. Methods that work in laboratory fail in real applications. The classical EIS approach[2] based on equivalent circuit models and DRT may be suitable for researchers, but has not yet shown its usability in commercial systems. New techniques are approaching like broadband excitation (e.g. PRBS) and nonlinear response analysis (NLRA) also referred to as THDA. And also the data analysis methodologies are changing. Key words are: relative wavelet entropy (RWP), continuous wavelet transform (CWT) or intermodular distortion analysis (IDA). Another point is the differentiation between data- and model-based approaches, it seems advantageous to combine both methods in hybrid approaches. As the price for powerful CPUs is steadily decreasing computational time-consuming methods can be utilized in on-line-monitoring systems. In hybrid approaches the algorithms can be differentiated by their execution time and memory demand: time consuming techniques might be used only with a slow rate or under specific operation conditions. The technological driving force for mass-market embedded systems with multicore CPU and floating-point units like for example the Infinion Aurix™ series is the growing complexity of automotive systems (key words are: Speech recognition, ADAS). Therefore, the implementation of complex, computational expensive, analytical models are in future realistic even in low cost monitoring systems. Beside the availability of embedded high-performance computational hardware, has the modernization of the tool chain to compute these embedded systems a huge impact. The development effort to compute FPGA hardware or control boards have been reduced dramatically by the introduction of tool boxes to transfer e.g. Matlab-code to platform compatible binary object files. Scientists do not longer rely on software engineers, which are skilled to code in basic languages like standard C or assembler. Therefore, the transition effort from the PC compatible code to embedded-system compatible code melts down. This has an impact on the complexity of upcoming monitoring algorithms.

[2] Excitation in the linear domain in compliance with the Kramers-Kronig-Theorem.